UNIVERSITY OF CALIFORNIA, SAN DIEGO

Nonlinear Silicon Photonics from the Near to Mid Infrared

A dissertation submitted in partial satisfaction of the requirements for the degree of

Doctor of Philosophy

in

Electrical Engineering (Photonics)

by

Jung Soo Park

Committee in Charge:

Professor Shayan Mookherjea, Chair
Professor Prabhakar R. Bandaru
Professor Dimitri N. Basov
Professor Joseph E. Ford
Professor Stojan Radic

2010

The Dissertation of Jung Soo Park is approved, and is acceptable in quality and form for publication on microfilm and electronically:

_____

_____

_____

_____

_____

Chair

University of California, San Diego

2010

DEDICATION

To my parents

EPIGRAPH

We choose to [do these] things, not because they are easy, but because they are hard,

because that goal will serve to organize and measure the best of our energies and skills,

because that challenge is one that we are willing to accept,

one we are unwilling to postpone,

and one which we intend to win.

-John F. Kennedy

TABLE OF CONTENTS

LIST OF ABBREVIATIONS

A_{eff}	Effective modal area
AFM	Atomic force microscopy
AM	Amplitude modulator
ASE	Amplified spontaneous emission
BOX	Buried oxide
BPF	Band pass filter
ChG	Chalcogenide glass
CMOS	Complementary metal-oxide-semiconductor
CROW	Coupled-resonator optical waveguide
CW	Continuous wave
DI	De-ionized
ECL	External cavity laser
EDFA	Erbium-doped fiber amplifier
FCA	Free-carrier absorption
FOM	Figure of merit
FOPA	Fiber-optic parametric amplifier

FOX	Flowable oxide
FWM	Four-wave mixing
Gb/s	Gigabit per second
GVD	Group velocity dispersion
HNLF	Highly-nonlinear fiber
HPF	High pass filter
HSQ	Hydrogen silsesquioxane
ICP/RIE	Inductively-coupled plasma reactive ion etching
IR	Infrared
LIDAR	Light detection and ranging
MIBK	Methyl isobutyl ketone
mW	Milliwatt
NIR	Near-infrared
OPO	Optical parametric oscillator
OSA	Optical spectrum analyzer
PBS	Polarizing beam splitter
PC	Polarization controller
PECVD	Plasma-enhanced chemical vapor deposition

PMMA	Poly (methyl methacrylate)
PM	Polarization maintaining
QCL	Quantum cascade laser
RF	Radio frequency
RIE	Reactive ion etching
sccm	Standard cubic centimeters per minute
SEM	Scanning electron microscopy
Si	Silicon
SiN	Silicon nitride
SiO_2	Silicon dioxide
SMF	Single-mode fiber
SOI	Silicon on insulator
SWIR	Short-wavelength infrared
TMAH	Tetramethylammonium hydroxide
TPA	Two-photon absorption
VOA	Variable optical attenuator
WDM	Wavelength division multiplexer
v_g	Group velocity

LIST OF FIGURES

LIST OF TABLES

ACKNOWLEDGEMENTS

I owe a great debt of gratitude to my advisor, Prof. Shayan Mookherjea, for his tremendous support throughout my graduate studies. Thanks to his advisement, guidance, encouragement, and hard work I was able to work on important problems that I was the most interested in, received expert advice in conducting my research, and also received invaluable personal advice that will stay with me throughout my future career. While working at Intel Labs leading up to the completion of my dissertation, I relied on the lessons that I learned directly from him nearly every day. He gave me every opportunity and all the resources to be successful that an advisor could give to a student, and only expected from me my very best, and for that I am grateful.

I also thank Prof. Stojan Radic, who co-supervised a great deal of the work presented in this dissertation, particularly on the parametric mixing experiments. Although he was not officially my advisor, he gave me an immense amount of encouragement and advice. He is responsible for many of the important lessons I learned through my graduate studies, and played a huge role in my successful graduate career, and for this I am grateful.

I am grateful to Sanja Zlatanovic, who worked tirelessly with me in the lab on the parametric mixing projects. We faced many enormous challenges in our work, and there were times when I admit that even I was unsure whether we would be successful. She refused to give up no matter what difficulties we faced, and her persistence and dedication was not only crucial to our work, but taught me extremely valuable personal lessons as well.

In the years that I shared a lab with Michael Cooper, I relied on his support numerous times. As the first two students in our group, there were many hurdles that we had to overcome in order to get anything done, but his dependable and steady presence made all the difference when times were the toughest. Whether it was the fourth quarter or overtime, I always knew I had a teammate I could count on. Other members of the Micro and Nano Photonics Group provided me great support over the years as well, including Mark Schneider, Greeshma Gupta, Yiran Shen, and Ben Ellis. From the Photonics Systems Lab I had great interactions with and received quite a bit of support from Nikola Alic, Jose Chavez-Boggio, Bill Kuo, Slaven Moro, Camille Brés, Andreas Wiberg, Evgeny Myslivets, Faezeh Gholami, Danny Blessing, Zeinab Taghavi, and JB Coles.

Prof. Prab Bandaru also helped me tremendously when I was starting out, and he and David Yang taught me many critical lessons in

device fabrication early on, which gave me a huge head start on my work. Additionally, my entire committee, including Prof. Joe Ford and Prof. Dimitri Basov (in addition to those already mentioned) gave me great advice in defining the topic of my dissertation.

Prof. Deli Wang, Prof. Ed Yu, Prof. Paul Yu, and Prof. Yuhwa Lo helped me get a head start when I first arrived at UCSD, along with Cesare Soci, Shadi Dayeh, Bin Xiang, Arthur Zhang, and David Aplin. They helped me gain my first experimental experience here and gave me guidance early on, which gave me a huge head start in discovering my research interests.

The staff of the Nano3 facilities at UCSD provided excellent support for my device fabrication work. I gratefully acknowledge Bernd Fruhberger, Ryan Anderson, Maribel Montero, Larry Grissom, Sean Parks, and Michael Clark for helping me in many ways. I gratefully acknowledge Ivan Divliansky (University of Central Florida) for his e-beam lithography contributions to my device fabrication, without which this work would not have been possible.

I am fortunate to have had many positive interactions with my fellow students, and have received great support and friendship from them over the years. I cannot possibly list every single one, but I am grateful to those including Winnie Chen, Wayne Chen, Arthur Zhang,

Sourobh Raychaudhuri, Shadi Dayeh, Jooyoung Song, Omer Lang, Steve Cho, Matt Pugh, Clay McPheeters, Colin Gage, Sy Sivaraman, Natan Jacobson, Sheu-Sheu Tan, David Yang, Maurice Ayauche, Anton Arriagada, Matt Chen, Johana Yan, Jessica Godin, Jeremy Law, Sunghwan Cho, Russell Burdt (and Rusty), Sam Yuspeh, Kate Baker, Jason Karp, Ryan Aguilnaldo, Jack Tzeng, Qing Gu, Marco Escobar-Acevedo, Maziar Nezhad, Swee Hoe Lim, Sangyeob Lee, and many others. Whether it was advice on research related or non-academic matters, serving on ECE Graduate Student Council or Graduate Student Association, or playing intramural sports, or simply enjoying being around San Diego, they helped make my graduate experience well-rounded, complete, and a lot more fun than I should probably admit in my dissertation. I also owe my thanks to the UCSD ECE student affairs staff, including Megan Scott, Gennie Miranda, Robert Rome, Terrance Mayes, Bernadette Villaluz, and Rachael Pope for their willingness to help in any administrative matters that I needed, as well as their vast efforts in improving graduate student life in our department.

Before completing my thesis, I was extremely fortunate to gain experience in an industry research lab as a member of the Photonics Technology Lab at Intel. I gratefully acknowledge those I have had the privilege to work with, including (but certainly not limited to) Ling Liao,

Haisheng Rong, Inho Kim, Juthika Basak, Vikram Sadagopan, Fred Haubensauk, Kuan-Pei Yap, Hyundai Park, Andy Hsieh, Brian Koch, Neil Na, and Mario Paniccia, just to name a few.

I gratefully acknowledge my funding sponsors who enabled my graduate studies. I received generous support from the UCSD ECE Department and the National Science Foundation Graduate Research Fellowship. I worked on projects funded by NSF, including a CAREER Award for Prof. Shayan Mookherjea, and DARPA.

Lastly, I gratefully acknowledge and thank my entire family, especially my parents to whom this dissertation is dedicated. Many relatives, distant and close, have been enormously supportive of me through the years. My sister has played such a key role in shaping the person that I am today while never letting me lose sight of the important things in life. The hard work and sacrifice of my parents to provide me the best future possible and all the opportunities that they never had themselves can never be adequately described, but there is not a single thing that I do that is possible without the undying love and support of my family.

Jung Park

La Jolla, CA

Chapter 2 contains material published in:

- S. Mookherjea, J. S. Park, S. H. Yang, P. R. Bandaru, "Localization in Silicon Nanophotonic Slow-Light Waveguides," *Nature Photonics*, **2** (2), 90 (2008)

The dissertation author contributed experimental work to the paper. The primary author planned and supervised the research, provided theoretical work, and assisted with experimental work and data analysis.

Chapters 3 and 4 contain, in part, material presented at:

- J. S. Park, S. Zlatanovic, M. L. Cooper, J. M. Chavez-Boggio, I. B. Divliansky, N. Alic, S. Mookherjea, S. Radic, "Two-Pump Four-Wave Mixing in Silicon Waveguides," *Frontiers in Optics: OSA 93rd Annual Meeting*, FML2, San Jose, 2009

The dissertation author was the primary author of the paper.

Chapter 5 contains material published in:

- S. Zlatanovic, J. S. Park, S. Moro, J. M. Chavez-Boggio, I. B. Divliansky, N. Alic, S. Mookherjea, S. Radic, "Mid-Infrared Wavelength Conversion in Silicon Waveguides Using Ultra-Compact Telecom-Band-Derived Pump Source," *Nature Photonics*, **4** (8), 561 (2010)

- J. S. Park, S. Zlatanovic, S. Moro, J. M. Chavez-Boggio, I. B. Divliansky, S. Mookherjea, S. Radic, "Mid-Infrared Four-Wave Mixing in Silicon Waveguides Using Telecom-Compatible Light Sources," *Frontiers in Optics: OSA 93rd Annual Meeting*, PDPB3, San Jose, 2009

The dissertation author is the co-primary author of the journal paper and was the presenter of the conference post-deadline session presentation.

VITA

2006	Bachelor of Science, Electrical Engineering
	University of California, Irvine
2007	National Science Foundation Graduate Research Fellow
2008	Master of Science, Electrical Engineering (Photonics)
	University of California, San Diego
2009	Candidate in Philosophy, Electrical Engineering (Photonics)
	University of California, San Diego
2010	Graduate Intern, Photonics Technology Lab, Intel Labs
	Intel Corporation, Santa Clara, CA
2010	Doctor of Philosophy, Electrical Engineering (Photonics)
	University of California, San Diego

PUBLICATIONS

C. Soci, A. Zhang, B. Xiang, S. A. Dayeh, D. A. Aplin, **J. Park**, X. Y. Bao, Y. H. Lo, D. Wang, "ZnO nanowire UV photodetectors with high internal gain," *Nano Letters*, **7** (4), 1003-1009 (2007)

A. Zhang, C. Soci, B. Xiang, **J. Park**, D. Wang, Y. H. Lo, "High gain ZnO nanowire phototransistor," *Conference on Lasers and Electro Optics*, (IEEE/OSA, Baltimore, MD, 2007)

C. Soci, B. Xiang, A. Zhang, **J. Park**, S. A. Dayeh, X. Y. Bao, Y. H. Lo, D. Wang, "Ultrahigh sensitivity ZnO UV detectors," *Materials Research Society Spring Meeting*, (MRS, San Francisco, CA, 2007)

S. Mookherjea, **J. S. Park**, S. H. Yang, P. R. Bandaru, "Light localization in silicon nanophotonic slow light waveguides," *Nature Photonics*, **2** (2), 90-93 (2008)

P. R. Bandaru, S. H. Yang, **J. S. Park**, S. Mookherjea, "Nanostructured silicon optical waveguides," *American Physical Society March Meeting*, (APS, New Orleans, LA, 2008)

S. H. Yang, P. R. Bandaru, M. L. Cooper, **J. S. Park**, S. Mookherjea, "Multi-slot optical waveguides, *Conference on Lasers and Electro Optics*, (IEEE/OSA, San Jose, CA, 2008)

J. S. Park, S. H. Yang, P. R. Bandaru, S. Mookherjea, "Light localization in silicon nanophotonic waveguides," *Conference on Lasers and Electro Optics*, (IEEE/OSA, San Jose, CA, 2008)

S. Mookherjea, M. L. Cooper, **J. S. Park**, S. H. Yang, P. R. Bandaru, "Design, fabrication, and measurement of giant birefringence at telecommunication wavelengths in multi-slotted silicon nanophotonic optical waveguides," *XXIX URSI General Assembly*, (URSI, Chicago, IL, 2008)

S. Mookherjea, **J. S. Park**, "Disorder and localization in microresonator arrays," *SPIE Photonics West: Laser Resonators and Beam Control XII*, (SPIE, San Jose, CA, 2009)

J. S. Park, S. Zlatanovic, M. L. Cooper, J. M. Chavez-Boggio, I. B. Divliansky, N. Alic, S. Mookherjea, S. Radic, "Two-pump four-wave mixing in silicon waveguides," *Frontiers in Optics*, (OSA, San Jose, CA, 2009)

J. S. Park, S. Zlatanovic, S. Moro, J. M. Chavez-Boggio, I. B. Divliansky, S. Mookherjea, S. Radic, "Mid-infrared four-wave mixing in silicon waveguides using telecom-compatible light sources," *Frontiers in Optics*, (OSA, San Jose, CA, 2009)

[Postdeadline Paper]

M. L. Cooper, G. Gupta, **J. S. Park**, M. A Schneider, I. B. Divliansky, S. Mookherjea, "Quantitative infrared imaging of SOI microring resonators," *Optics Letters*, **35** (5), 784-786 (2010)

G. Gupta, M. L. Cooper, **J. S. Park**, M. A. Schneider, W. H. Steier, S. Mookherjea, "Tuning of microring resonators" Proc. SPIE, Vol. 7612, 76120Q, *Photonics West* (SPIE, San Francisco, CA, 2010)

M. L. Cooper, G. Gupta, **J. S. Park**, M. A. Schneider, I. B. Divliansky, S. Mookherjea, "Characterization of SOI microrings using IR imaging," *Conference on Lasers and Electro Optics*, (IEEE/OSA, San Jose, CA, 2010)

S. Zlatanovic[1], **J. S. Park**[1], S. Moro, J. M. Chavez-Boggio, I. B. Divliansky, N. Alic, S. Mookherjea, S. Radic, "Mid-infrared wavelength conversion in silicon waveguides using ultra-compact telecom-band-derived pump source," *Nature Photonics*, **4** (8), 561-564 (2010)

[[1]equal contribution]

ABSTRACT OF THE DISSERTATION

Nonlinear Silicon Photonics from the Near to Mid Infrared

by

Jung Soo Park

Doctor of Philosophy in Electrical Engineering (Photonics)

University of California, San Diego, 2010

Professor Shayan Mookherjea, Chair

This dissertation presents experimental work investigating silicon-on-insulator (SOI) photonic waveguides for parametric nonlinear optic devices. An introduction is presented in Chapter 1, including background and motivation for exploring SOI as a platform for integrated photonics, as well as an overview of integrated nonlinear optic devices. Chapter 2 discusses on-chip slow light structures based on coupled-resonator optical waveguides (CROW), potentially useful for enhancing nonlinearities for efficient chip-scale nonlinear optics. Although slowing light is limited by

fabrication tolerance-induced disorder, a fundamental phenomenon is observed: the Anderson localization of optical waves.

Chapter 3 of the dissertation discusses four-wave mixing in SOI waveguides. SOI waveguide fabrication is described in detail, including achieving low fiber-to-chip coupling loss and waveguide propagation loss. Two approaches for dispersion engineering are presented: with the design of waveguide dimensions and with a thin-film cladding. Parametric wavelength conversion by degenerate (single-pump) FWM in these dispersion-engineered waveguides is demonstrated and discussed.

Chapter 4 concerns FWM with two pumps, an approach that promises functionalities not possible with a single pump such as multiple sideband generation with self-seeded higher-order pumps. In addition to demonstrating the generation of up to ten sidebands with dual pumps and subsequent self-seeded higher order pumps, we characterize trade-offs in maximum conversion efficiency due to nondegenerate two-photon absorption (TPA).

The work presented in Chapter 5 takes a novel approach to SOI parametric devices by exploring a new spectral range, toward the mid-infrared (mid-IR), near 2 μm and beyond. We measure FWM in silicon waveguides with a pump near 2 μm, which itself is generated by the parametric conversion of a 1300 nm seed by a 1589 nm pump in a highly-

nonlinear fiber (HNLF). Fundamentally, our results show promising nonlinear properties of silicon waveguides near 2 μm, as the generation of a record-long wavelength from a first-order parametric conversion in a waveguide of 2388 nm is achieved. This result also demonstrates promise for a new class of mid-IR light sources constructed from sources and components that are telecom-compatible, and hence widely available.

1. INTRODUCTION

1.1 Introduction to Silicon Photonics

There is a vast and aggressive effort taking place to miniaturize and densely integrate photonic devices on a chip-scale platform, with significant focus on silicon photonics in the past decade, largely driven by such applications as optical interconnects for electronic circuits (Fig 1.1) [1, 2]. This push for CMOS-compatible photonic circuits for microprocessor interconnect applications is evident not only by tremendous effort around the scientific and academic research community, but also by large computing corporations including Intel, Hewlett Packard, Sun Microsystems/Oracle, and IBM. The silicon-on-insulator (SOI) platform, where single-crystal silicon forms a device layer isolated from the bulk wafer by a layer of oxide, offers many advantages that makes it the obvious choice as an integrated optical interconnects platform for several reasons. From the standpoint of optical waveguides, SOI provides the highest refractive index contrast of any commonly available and wafer-scale manufacturable transparent dielectric material in the near infrared (telecommunication-compatible) spectral range, with the index contrast between silicon and silicon dioxide being $\Delta n \approx 2$. The tight optical confinement provided by such index contrast allows for very small

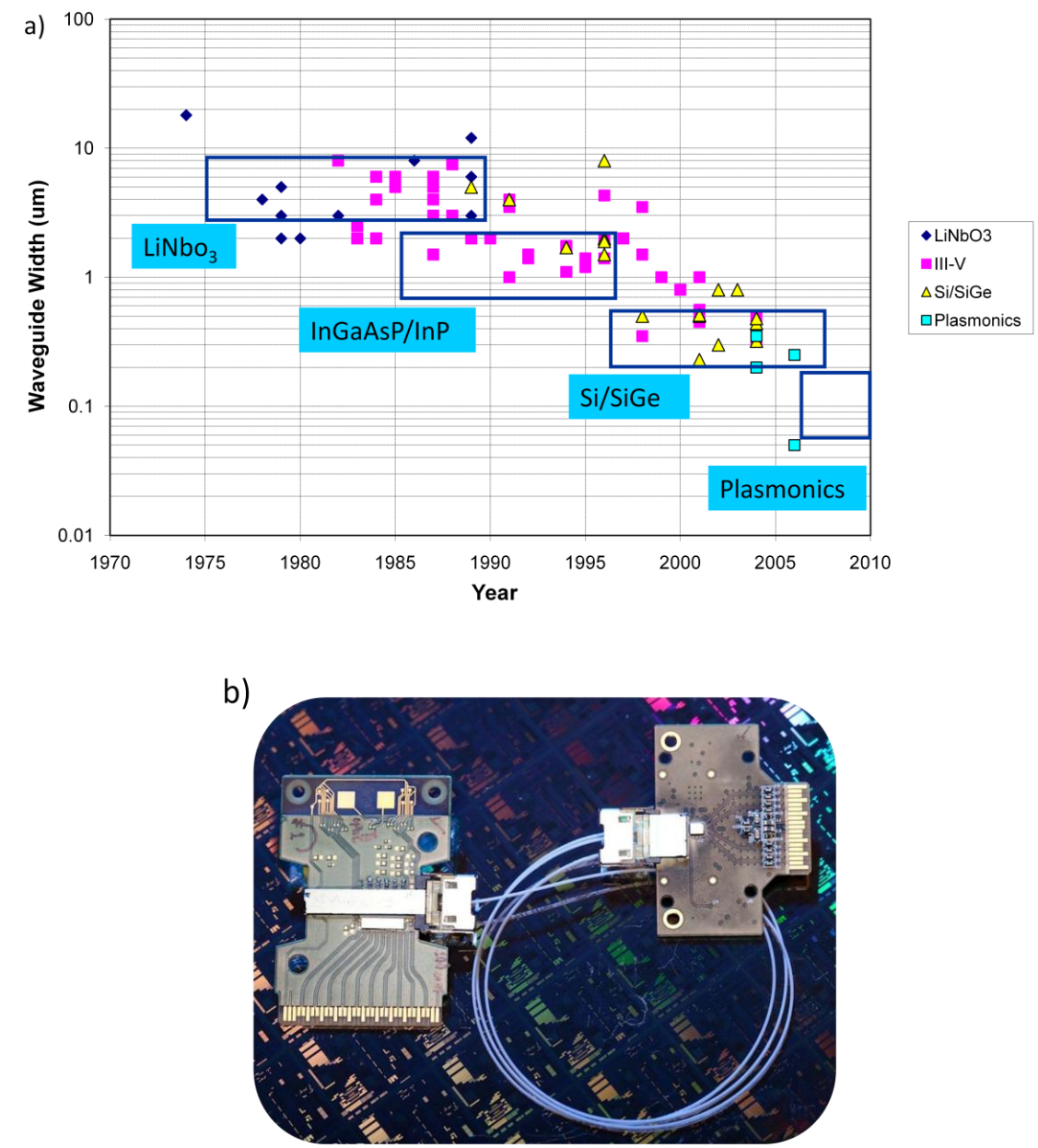

Figure 1.1: Trends in waveguide scaling. a) Research in dielectric waveguides has led to scaling to sub-micron dimensions, enabled by the high index contrast provided by the SOI materials platform. b) A fully integrated silicon photonics chip developed by Intel Labs including III-V hybrid laser, silicon modulator, wavelength multiplexers, on the transmitter and a SiGe detector and trans-impedance amplifier on the receiver. Photo credit: Intel Corporation.

waveguide bend radii, and thus very small device footprints, essential for dense integration and not offered by polymer or high-index-glass based platforms. From a practical standpoint, silicon is a much more affordable and abundant material than its III-V semiconductor counterparts, while the maturity of silicon fabrication technology is unparalleled thanks to decades of development by the CMOS electronics industry. Plasmonic waveguides offer extremely small device footprint, but the high propagation losses imply unreasonable power requirements.

While silicon has these advantages, there are disadvantages as well, including no direct electrically-pumped light emission and no electro-optic effect, extreme sensitivity to fabrication tolerances due to high index contrast, and strict materials and processing constraints of the CMOS foundry. Issues specific to SOI include thermal issues during processing due to the BOX leading to thermal expansion and strain, and relatively high wafer cost compared to standard silicon wafers. Despite these engineering challenges, SOI photonic devices remain a key candidate for many important applications.

Consequently, this push for silicon photonic devices has also led to advances in integrated photonics for a wide variety of applications, including nonlinear optic devices [45] for applications such as Raman amplifiers and lasers [3, 4], all-optical nonlinear switching [5, 6], time-to-

frequency domain transformation and manipulation [7, 8], and high-speed optical sampling [9]. Silicon has a high nonlinear refractive index n_2 (three orders of magnitude higher than silica glass), and tight modal confinement in SOI waveguides (modal effective area A_{eff} two orders of magnitude smaller than single-mode optical fiber), which provide huge enhancement in the nonlinearity coefficient $\gamma \propto n_2/A_{eff}$ [10, 36]. SOI is therefore a highly attractive platform for engineering nonlinear optic devices. However, along with high (real $\chi^{(3)}$) nonlinearity, silicon comes with high nonlinear absorption (imaginary $\chi^{(3)}$) from two-photon absorption (TPA) and the resulting free-carrier absorption (FCA). It is important to study these trade-offs and characterize the performance of SOI nonlinear optic devices. This chapter will review the current state of integrated nonlinear photonic devices, and provide an outline to the forthcoming dissertation chapters.

1.2 Parametric Nonlinear Optics in Integrated Photonics

1.2.1 Introduction to Parametric Nonlinear Optics

Optical nonlinearities occur when the nonlinear terms of the material polarizability must be accounted for, and are classified according those induced by the second or third-order nonlinear susceptibilities, $\chi^{(2)}$ and $\chi^{(3)}$, respectively. In this dissertation we focus on

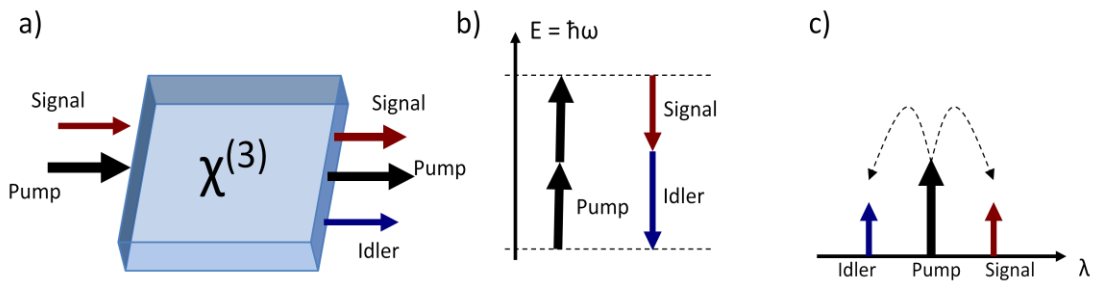

Figure 1.2: Four-wave mixing illustration. a) Schematic of the four-wave mixing interaction in which a pump and signal mix in a $\chi^{(3)}$ medium to generate an idler wave. b) Energy-level description of the FWM process showing two pump photons giving their energy to generate one photon each at the signal and idler frequencies. c) Four-wave mixing illustrated in wavelength.

nonlinear optical interactions arising from the third order nonlinear susceptibility $\chi^{(3)}$, which is the lowest order nonlinearity in centrosymmetric materials such as silicon. It is through $\chi^{(3)}$that waves of different frequencies propagating in a medium can interact with the medium and each other, exchange energy, and generate waves at new frequencies; the distinct difference from any linear system. Of particular interest is four-wave mixing (FWM), a parametric process in which the interaction of a pump and probe (or signal) through $\chi^{(3)}$generates an idler wave whose frequency is equal to the difference between twice the pump frequency and the probe frequency (in general, the term "parametric" refers to processes in which the initial and final quantum mechanical states are the same) [11]. The FWM process is illustrated in Fig 1.2. Two pump photons

give their energy to create one photon at each the probe frequency and idler frequency. As a result, the pump converts, or copies, the probe to the idler.

Many all-optical signal processing applications are based on the FWM interaction. One practical and widely used device is the parametric amplifier, including fiber-optic parametric amplifiers (FOPA), which is simply a nonlinear material (such as a section of optical fiber) in which a pump and signal are inserted, such that the pump amplifies the signal while converting the signal to an idler [12]. Proper engineering of the pump source and the fiber can provide very high gain over very broad bandwidths [13]. FOPAs are especially useful not only as amplifiers, but also by providing coherent light sources and parametric amplification either across bandwidths which no materials-gain medium such as erbium-doped devices can cover, or at wavelengths in which lasers or amplifiers are not widely available. For example, they can translate near-infrared sources, which are very-well developed and affordable thanks to the fiber optics telecommunications industry, to the visible wavelength range [14], or to longer wavelengths in the short-wave infrared [15]. Additionally, FWM been used in both fiber and integrated devices for a variety of applications including phase conjugation for dispersion compensation [16], multicasting and ultra-high data rate sampling [17-19],

frequency comb generation [20], optical delays with extremely large delay-bandwidth products [21], signal regeneration [22, 23] and time-to-frequency domain transformation and manipulation [7, 24].

1.2.2 Integrated Nonlinear Optics Platforms

Many of the most advanced signal processing tools afforded by parametric processing thus far have been most well-developed in optical fiber [12], while nonlinear optics in bulk crystals has also been studied extensively [25]. The constant push for chip-scale integration, however, demands investigation into integrated platforms for parametric processing. The preferred candidates thus far include a variety of semiconductors including III-V materials, chalcogenide glass (ChG), polymers, high-index doped glass, as well as SOI. The important nonlinear parameters to consider are the nonlinearity coefficient γ, the nonlinear refractive index n_2, and the intensity-dependent absorption (TPA) coefficient β_2, which are related to the third-order nonlinear susceptibility $\chi^{(3)}$ by [12]

$$n_2 = \frac{3Z_0 Re\{\chi^{(3)}\}}{4n_0^2} \tag{1.1}$$

$$\beta_2 = \frac{3k_0 Z_0 Im\{\chi^{(3)}\}}{2n_0^2}. \quad (1.2)$$

Table 1.1 compares the nonlinearity of silicon to other materials. Of these materials, silicon is the preferred material of choice due to increased nonlinearity and mature fabrication technology over nonlinear glasses [26]. Although various polymers have been shown to have high nonlinearity, silicon provides higher index contrast, thermal stability, and long-term stability over these organic materials.

Table 1.1: Nonlinear properties of integrated photonics materials. Comparison of the nonlinearity coefficients of silicon, glass, and organic polymer materials

Material	Re{γ} [(Wm)$^{-1}$]	λ [nm]	n_0	n_2 [m^2/W]	Ref.
Silicon	406	1550	3.48	5 x 10^{-18}	35
	365	1540	3.48	4.5 x 10^{-18}	36
	487	1550	3.48	6 x 10^{-18}	37
Inorganic Materials					
Pure silica	0.5	1550	1.45	2.48x10^{-20}	12
Chalcogenide glass	86	1600	2.45	1x10^{-17}	38
	117	1500	2.81	2.3x10^{-17}	39
Bismite glass	4.4	1550	2.02	3.2x10^{-19}	40
Tellurite glass	7.5	1900	2.2	6.5x10^{-19}	41
Organic Materials					
PSTF66	54	1550	1.5	2.8x10^{-18}	42
PDA	92	1319	1.5	4.8x10^{-18}	43
PTS	3820	1600	1.7	2.2x10^{-16}	44

1.2.3 Progress in SOI Nonlinear Optics

Optical amplifiers in silicon have been demonstrated based on the Raman scattering effect, including pulsed [3] and continuous-wave [4] lasers, short-wavelength infrared lasers [27], and mid-infrared amplifiers [28]. Even though these devices exhibit large gain and lasing capability, the Raman scattering process has a very narrow bandwidth of roughly 1 nm [29], which inherently limits its usefulness to most signal processing functionalities beyond amplification and lasing. The FWM process can be engineered with proper phase matching conditions to cover very large bandwidths exceeding 100 nm in optical fiber [13] and even much wider in SOI waveguides [30]. Hence, there has been a large effort in achieving efficient and broad-band FWM in SOI waveguides.

FWM has been demonstrated in silicon waveguides by a number of research groups. Reported results in the telecommunications band near 1550 nm include up to -5.5 dB continuous-wave conversion efficiency [31], conversion of 40GB/s [32] or higher [33] data and parametric gain using a ultra-short pulse pump source [34]. Table 1.2 lists reported FWM conversion efficiencies achieved thus far.FWM in silicon have enabled a wide range of all-optical signal processing capabilities including, photonic "time lens" [7, 24] and ultra-high data rate multicasting and sampling [19, 9].

Table 1.2: Four-wave mixing conversion efficiencies in literature. Survey of four-wave mixing conversion efficiency achieved in literature

Report	Waveguide W x H (nm x nm)	Conversion Efficiency	Pump
Columbia/IBM – OpEx **13** (11) p4341 (2005)	220 x 445	-21 dB	CW
NTT – OpEx **13** (12) p4629 (2005)	200 x 400 w/ SiO_yN_x cladding	-35 dB	CW
Intel – OpPex **14** (24) p11721 (2006)	1550 x 1500 rib with 700 nm etch depth	-8.68 dB	CW, reverse-bias p-i-n
Intel – OpPex **16** (21) p16735 (2008)	600 x 340, 130 nm etch depth	-5.5 dB	CW
Cornell – Nature **441** p960 (2006)	300 x 550 to 300 x 600	+5.2 dB	3.5 ps pulsed pump (2-12 W peak)
Cornell – OpEx **15** (20) p12949 (2007)	300 x 500 to 300 x 750	-12 dB	CW
Columbia/IBM – Nature Photonics **4** (8) p557 (2010)	425 x 700	+25.4	Mid-infrared pump (2200 nm), 2 ps pump pulses

Despite these advances, many fundamental and practical challenges remain in developing practical nonlinear silicon photonic devices, of which this dissertation attempts to address a few key issues. The first is the high pump power requirement for many useful FWM applications, which so far has required off-chip sources and amplifiers, often offsetting the advantage of small device footprint of SOI devices. This may be improved upon through enhanced nonlinearities by slowing the propagation of light and increasing light-matter interaction [46, 47]. Also, non-degenerate FWM with multiple pumps may yield functionalities not achievable with a single pump, and warrants investigation. Lastly,

while current progress has been largely dominated by work in the telecommunications window near 1550 nm, many important applications of photonic devices rely on mid-infrared light sources, such as chemical and biomolecular sensing, free-space communication and atmospheric sensing, and infrared spectroscopy. The large nonlinearity of silicon combined with the reduction or absence of nonlinear absorption normally suffered in the near-infrared may make silicon an attractive platform for mid-infrared nonlinear optics. This dissertation seeks to address these open issues through experimental research in silicon guided-wave nonlinear devices.

1.3 Outline of the Dissertation

The dissertation is organized as follows: Chapter 2 discusses slow light in silicon photonics, which is partially motivated by promise for efficient chip-scale nonlinear interactions. We instead demonstrate that although slow light limitations due to practical fabrication tolerances are severe, Anderson localization of light is observed, a fundamental phenomenon that occurs due to variation and weak disorder that is unavoidable in any fabrication process. Chapter 3 discusses FWM in straight SOI waveguides. In order to achieve FWM in silicon, low fiber-to-chip coupling loss and low waveguide propagation loss are required.

These are described in detail, as they affect all device fabrication for the rest of the thesis. Chapter 4 presents dual-pump FWM in silicon waveguides. Non-degenerate and degenerate FWM and nonlinear absorption are compared. Chapter 5 investigates the nonlinear properties of SOI waveguides near the mid-infrared spectral region, in contrast to the telecommunication band in the near-infrared. Chapter 6 concludes the dissertation and proposes possible future work based on the work presented.

REFERENCES

[1] D. A. B. Miller, "Device requirements for optical interconnects to silicon chips," *Proceedings of the IEEE*, **97** (7), 1166 (2009)

[2] R. Won, "Simply Silicon," *Nature Photonics*, **4** (8), 498 (2010)

[3] O. Boyraz, B. Jalali, "Demonstration of a silicon Raman laser," *Optics Express*, **12** (21), 5269 (2004)

[4] H. Rong, R. Jones, A. Liu, O. Cohen, D. Hak, A. Fang, M. Paniccia, "A continuous-wave Raman silicon laser," *Nature*, **433**, 725 (2005)

[5] K. Ikeda, "All-optical nonlinear switching in optical micro-resonators on a silicon chip," PhD Dissertation, University of California, San Diego, 2008

[6] M. Notomi, A. Shinya, S. Mitsugi, G. Kira, E. Kuramochi, T. Tanabe, "Optical bistable switching action of Si high-Q photonic-crystal nanocavities," *Optics Express*, **13** (7), 2678 (2005)

[7] D. R. Solli, J. Chou, B. Jalali, "Amplified wavelength-time transformation for real-time spectroscopy," *Nature Photonics*, **2** (1), 48 (2008)

[8] M. A. Foster, R. Salem, D. F. Geraghty, A. C. Tuner-Foster, M. Lipson, A. L. Gaeta, "Silicon-chip-based ultrafast oscilloscope," *Nature*, **456**, 81 (2008)

[9] R. Salem, M. A. Foster, A. C. Turner-Foster, D. F. Geraghty, M. Lipson, A. L. Gaeta, "High-speed optical sampling using a silicon-chip temporal magnifier," *Optics Express*, **17** (6), 4324 (2009)

[10] C. Koos, L. Jacome, C. Poulton, J. Leuthold, W. Freude, "Nonlinear silicon-on-insulator waveguides for all-optical signal processing," *Optics Express*, **15** (10), 5976 (2007)

[11] R. Boyd, *Nonlinear Optics*, 3rd Ed, Academic Press, Burlington, MA, 2008

[12] G. P. Agrawal, *Nonlinear Fiber Optics*, 4th Ed, Academic Press, Burlington, MA, 2007

[13] J. M. Chavez-Boggio, J. D. Marconi, S. R. Bickham, H. L. Fragnito, "Spectrally flat and broadband double-pumped fiber optical parametric amplifiers," *Optics Express*, **15** (9), 5288 (2007)

[14] R. Jian, R. E. Saperstein, N. Alic, M. Nezhad, C. J. McKinstrie, J. E. Ford, Y. Fainman, S. Radic, "Continuous-wave band translation between the near-infrared and visible spectral ranges," *Journal of Lightwave Technology*, **25** (1), 58 (2007)

[15] J. M. Chavez-Boggio, S. Zlatanovic, F. Gholami, J. M. Aparicio, S. Moro, K. Balch, N. Alic, S. Radic, "Short wavelength infrared frequency conversion in ultra-compact fiber device," *Optics Express*, **18** (2), 439 (2010)

[16] E. Myslivets, B. P. P. Kuo, A. O. Wiberg, S. Zlatanovic, S. Moro, F. Gholami, A. Peric, C. S. Brés, N. Alic, S. Radic, "Transmission of 640 Gbps RZ-OOK channel over 100 km of SSMF by wavelength-transparent conjugation," *Optical Fibers Conference*, PDPC6 (IEEE/OSA, San Diego, CA, 2010)

[17] C. S. Brés, A. O. J. Wiberg, B. P. P. Kuo, J. M. Chavez-Boggio, C. F. Marki, N. Alic, S. Radic, "Optical demultiplexing of 320 Gb/s to 8-times-40 Gb/s in a single parametric gate," *Journal of Lightwave Technology*, **28** (4), 434 (2010)

[18] A. O. J. Wiberg, C. S Brés, B. P. P. Kuo, J. X. Zhao, N. Alic, S. Radic, "Sampling of Multiple 320-Gb/s Channels by Single Parametric Gate," *IEEE Photonics Technology Letters*, **21** (12), 796 (2009)

[19] A. Biberman, B. G. Lee, K. Bergman, A. C. Turner-Foster, M. Lipson, M. A. Foster, A. L. Gaeta, "First Demonstration of On-Chip Wavelength Multicasting," *Optical Fibers Conference* (IEEE/OSA, San Diego, CA, 2009)

[20] J. M. Chavez-Boggio, S. Moro, N. Alic, S. Radic, "Nearly octave-spanning cascaded four-wave mixing generation in low-dispersion highly nonlinear fiber," *Proceedings of European Conference on Optical Communication* (Vienna, Austria, 2009)

[21] E. Myslivets, N. Alic, S. Moro, B. P. P. Kuo, R. M. Jopson, C. J. McKinstrie, M. Karlsson, S. Radic, "1.56μs Continuously tunable parametric delay line for a 40-Gb/s signal," *Optics Express*, **17** (14), 11958 (2004)

[22] K. K. Chow, C. Shu, Chinlon Lin, A. Bjarklev, "All-Optical Signal Regeneration Based on Pump-Modulated Four-Wave Mixing in a Nonlinear Photonic Crystal Fiber," *Conference on Lasers and Electro Optics* (IEEE/OSA, Baltimore, MD, 2005)

[23] R. Salem, M. A. Foster, A. C. Turner, D. F. Geraghty, M. Lipson, A. L. Gaeta, "Signal regeneration using low-power four-wave mixing on silicon chip," *Nature Photonics*, **2** (1), 35 (2008)

[24] M. A. Foster, R. Salem, Y. Okawachi, A. C. Tuner-Foster, M. Lipson, A. L. Gaeta, "Ultrafast waveform compression using a time-domain telescope," *Nature Photonics*, **3**, 581 (2009)

[25] D. N. Nikogosyan, *Nonlinear Optical Crystals, a Complete Survey*, Springer, New York, NY, 2005

[26] M. Ferrera, L. Razzari, D. Duchesne, R. Morandotti, Z. Yang, M. Liscidini, J. E. Sipe, S. Chu, B. E. Little, D. J. Moss, "Low-power continuous-wave nonlinear optics in doped silica glass integrated waveguide structures," *Nature Photonics*, **2**, 737 (2008)

[27] H. Rong, S. Xu, O. Cohen, O. Raday, M. Lee, V. Sih, M. Paniccia, "A cascaded silicon Raman laser," *Nature Photonics*, **2** (3), 170 (2008)

[28] V. Raghunathan, D. Borlag, R. R. Rice, B. Jalali, "Demonstration of a mid-infrared silicon Raman amplifier," *Optics Express*, **15** (22), 14355 (2007)

[29] R. Claps, D. Dimitropoulos, V. Raghunathan, Y. Han, B. Jalali, "Observation of stimulated Raman amplification in silicon waveguides," *Optics Express*, **11** (15), 1731 (2003)

[30] A. C. Turner-Foster, M. A. Foster, R. Salem, A. L. Gaeta, M. Lipson, "Frequency conversion over two-thirds of an octave in silicon nanowaveguides," *Optics Express*, **18** (3), 1904 (2010)

[31] W. Mathlouthi, H. Rong, M. Paniccia, "Characterization of efficient wavelength conversion by four-wave mixing in sub-micron silicon waveguides," *Optics Express*, **16** (21), 16735 (2008)

[32] Y. H. Kuo, H. Rong, V. Sih, S. Xu, M. Paniccia, O. Cohen, "Demonstration of wavelength conversion at 40 Gb/s data rate in silicon waveguides," *Optics Express*, **14** (24), 11721 (2006)

[33] F. Li, M. Pelusi, D-X. Xu, A. Densmore, R. Ma, S. Janz, D.J. Moss, "Error-free all-optical demultiplexing at 160 Gb/s via FWM in a silicon nanowire," *Optics Express*, **18** (4), 3905 (2010)

[34] M. A. Foster, A. C. Turner, J. E. Sharping, B. S. Schmidt, M. Lipson, A. L. Gaeta, "Broad-band optical parametric gain on a silicon photonic chip," *Nature*, **440**, 960 (2006)

[35] E. Dulkeith, Y. A. Vlasov, X. Chen, N. C. Panoiu, R. M. Osgood, "Self-phase modification in submicron silicon-on-insulator photonic wires," *Optics Express*, **14**, 5524 (2006)

[36] M. Dinu, F. Quochi, H. Garcia, "Third-order nonlinearities in silicon at telecom wavelengths," *Applied Physics Letters*, **82** (18), 2954 (2003)

[37] H. K. Tsang, C. S. Wong, T. K. Liang, I. E. Day, S. W. Roberts, A. Harpin, J. Drake, M. Asghari, "Optical dispersion, two-photon absorption and self-phase modification in silicon waveguides at 1.5 μm wavelength," *Applied Physics Letters*, **80** (3), 416 (2002)

[38] T. Cardinal, K. A. Richardson, H. Shim, A. Schulte, R. Beatty, K. Le Fougoc, C. Meheghini, J. F. Viens, A. Villeneuve, "Non-linear properties of chalcogenide glasses in the system As-S-Se," *Journal of Non-Crystalline Solids*, **256-257**, 353 (1999)

[39] J. M. Harbold, F. Ö. Ilday, F. W. Wise, J. S. Sanghera, V. Q. Nguyen, L. B. Shaw, I. D. Aggarwal, "Highly nonlinear As-S-Se glasses for all-optical switching," *Optics Letters*, **27** (2), 119 (2002)

[40] K. Kikuchi, K. Taira, N. Sugimoto, "Highly nonlinear bismuth oxide-based glass fibers for all-optical signal processing," *Electronics Letters*, **38** (4), 166 (2002)

[41] H. Nasu, O. Matsushita, K. Kamiya, H. Kobayashi, K. Kubodera, "Third harmonic generation from Li2-TiO2-TeO2 glasses," *Journal of Non-Crystalline Solids*, **124** (2-3), 275 (1990)

[42] M. Asobe, I. Yokohama, T. Kaino, S. Tomaru, T. Kurihara, "Nonlinear absorption and refraction in an organic dye functionalized main chain polymer waveguide in the 1.5 μm wavelength region," *Applied Physics Letters*, **67** (7), 891 (1995)

[43] K. Rochford, R. Zanoni, G. I Stegeman, W. Krug, E. Miao, M. W. Beranek, "Measurement of nonlinear refractive index and transmission in polydicetylene waveguides at 1.319 μm," *Applied Physics Letters*, **58** (1), 13 (1991)

[44] B. L. Lawrence, M. Cha, J. U. Kang, W. Toruellas, G. Stegeman, G. Baker, J. Meth, S. Etemad, "Large purely refractive nonlinear index of single crystal p-toluene-sulphonate (PTS) at 1600 nm," *Electronics Letters*, **30** (5), 447 (1994)

[45] J. Leuthold, C. Koos, W. Freude, "Nonlinear silicon photonics," *Nature Photonics*, **4** (8), 535 (2010)

[46] B. Corcoran, C. Monat, C. Grellet, D. J. Moss, B. J. Eggleton, T. P. White, L. O'Faolain, T. F. Krauss, "Green light emission in silicon through slow-light enhanced third-harmonic generation in photonic-crystal waveguides," *Nature photonics*, **3** (4), 206 (2009)

[47] Y. Chen, S. Blair, "Nonlinearity Enhancement in Finite Coupled-Resonator Optical Waveguides," *Optics Express*, **12** (15), 3353 (2004)

2. SLOW LIGHT AND LIGHT LOCALIZATION IN SILICON PHOTONICS

2.1 Coupled-Resonator Optical Waveguides

Aside from being one of the most interesting fundamental challenges in current photonics research, slow light could have significant technological impact, providing optical delays and buffers for applications including all-optical signal processing and optical interconnects. A seemingly contradictory effort to slow the propagation of light in order to boost the speed of computer processor interconnects has been actively pursued using a variety of techniques including photonic crystal waveguides and coupled microresonators [1-3, 18]. While slow light is of interest to optical interconnects applications as optical delays and buffers, it is also of great interest to resonantly-enhanced chip-scale nonlinear optics. Slowing the propagation of light enhances its interaction with the material, promising optical nonlinearities with significantly higher efficiency and lower power requirements. As the expected enhancement in nonlinearity scales inversely with the group velocity squared $(1/{v_g}^2)$ [4], slow light could be key to the realization of efficient integrated nonlinear devices.

One attractive approach to slow light on chip is with coupled-resonator optical waveguides (CROW), composed of a periodic

sequence of cascaded optical microresonators (Fig 2.1) [5]. CROWs are attractive for slow-light devices for a variety of reasons. First, they utilize structural properties rather than materials properties to slow light, thus

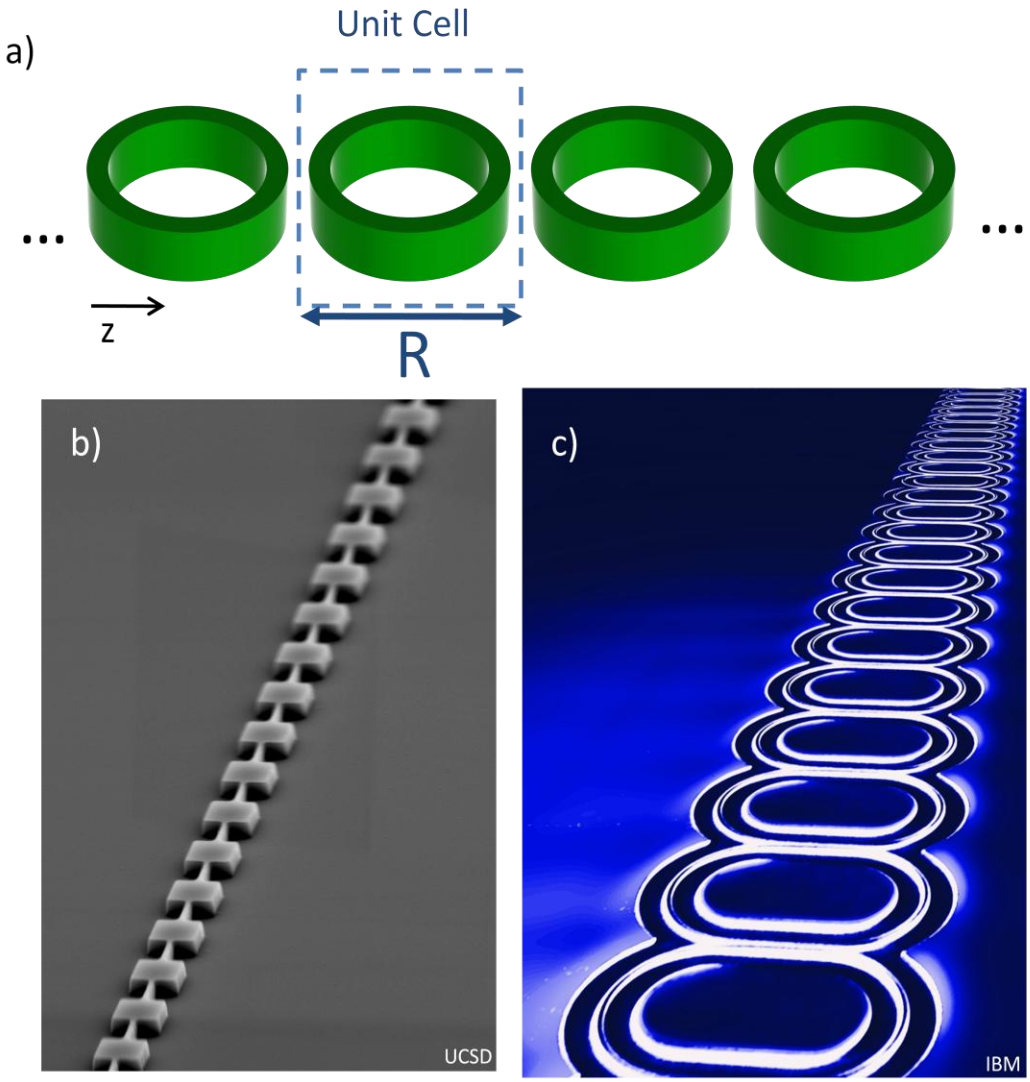

Figure 2.1: Coupled-resonator optical waveguides. a) Schematic of a CROW composed of microring resonators. b) CROW composed of square resonators (ref. 7 and discussed in this chapter). c) CROW fabricated by IBM (ref. 18) Image of Photonics, Courtesy of International Business Machines Corporation

materials resonances are not required. This is especially useful for SOI, where neither strong absorption resonances nor material gain is available in any spectral region of interest, and fortunately are not required. Secondly, any standard evanescently-coupled microresonator can be a building block for a CROW, including microring and microdisk resonators and photonic crystal microcavities. Devices composed of standard building blocks are attractive for practical purposes, especially for large-scale integration.

Light propagation in a CROW is most simply described by computing its dispersion using the tight binding approximation [5]. The CROW eigenmode $\boldsymbol{E}_K(\boldsymbol{r}, t)$ is a linear combination of the individual resonator eigenmodes $\boldsymbol{E}_\Omega$

$$\vec{E}_K(\vec{r}, t) = E_0 e^{i\omega_k t} \sum_{n,\Omega} e^{inKR} b_\Omega \vec{E}_\Omega(\vec{r} - nR\hat{z}) \quad (1)$$

which satisfies the wave equation

$$\nabla \times \left(\nabla \times \vec{\mathrm{E}}_\mathrm{K}\right) = \epsilon(\vec{\mathrm{r}}) \frac{\omega_\mathrm{K}^2}{\mathrm{c}^2} \vec{\mathrm{E}}_\mathrm{K} \quad (2)$$

where Ω is the single-resonator eigenfrequency. Substituting (1) into (2), multiplying both sides by $\boldsymbol{E}_{\Omega}$, and spatially integrating yields the dispersion relation ω as a function of K, given as

$$\omega_K^2 = \frac{\left[1+\sum_{n\neq 0} e^{-inKR}\beta_n\right]}{\left[1+\delta\alpha+\sum_{n\neq 0} e^{-inKR}\alpha_n\right]} \tag{3}$$

where the overlap integrals α_n, β_n, and $\delta\alpha$ are given by

$$\alpha_n = \int d^3\vec{r}\,\epsilon(\vec{r})\vec{E}_{\Omega}\cdot\vec{E}_{\Omega}(\vec{r}-nR\hat{z}), \qquad n\neq 0 \tag{4}$$

$$\beta_n = \int d^3\vec{r}\,\epsilon(\vec{r}-nr\hat{z})\vec{E}_{\Omega}\cdot\vec{E}_{\Omega}(\vec{r}-nR\hat{z}), \qquad n\neq 0 \tag{5}$$

$$\delta\alpha = \int d^3\vec{r}\,[\epsilon(\vec{r})-\epsilon_0(\vec{r})]\vec{E}_{\Omega}\cdot\vec{E}_{\Omega}. \tag{6}$$

The tight binding approximation assumes nearest-neighbor coupling only, such that the expressions (4-6) only have non-zero value when $n = \pm 1$. This simplifies the dispersion to a simple cosine relation

$$\omega(K) = \Omega\left[1-\frac{\delta\alpha}{2}+\kappa_1\cos(KR)\right] \tag{7}$$

where the nearest-neighbor coupling coefficient κ is given by

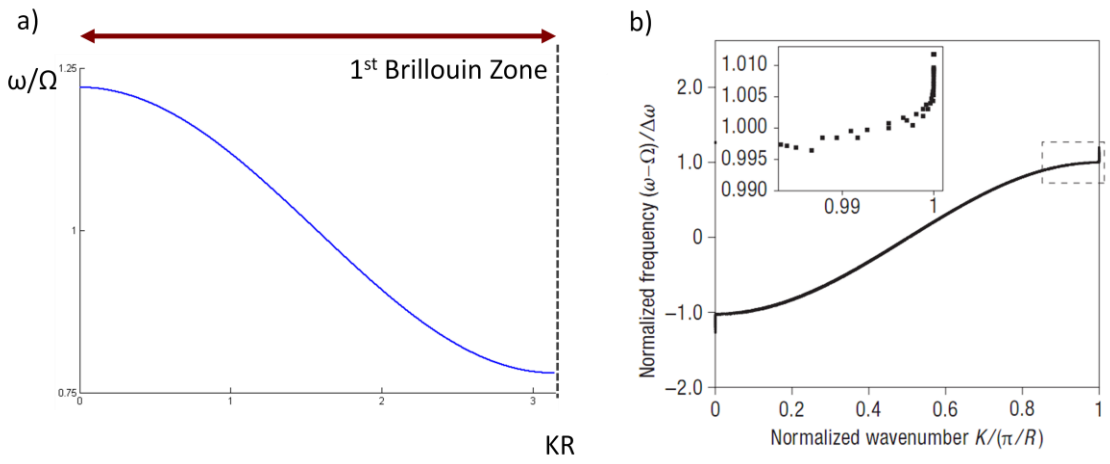

Figure 2.2: CROW dispersion. a) Calculated dispersion of an ideal CROW follows a cosine expression (Eq. 7) with flat dispersion at the edges of the first Brillouin zone. b) Calculated dispersion of a CROW with 1% variation in the nearest-neighbor coupling coefficient

$$\kappa_1 = \beta_1 - \alpha_1 = \int d^3\vec{r}\,[\epsilon_0(\vec{r} - R\hat{z}) - \epsilon(\vec{r} - R\hat{z})]\vec{E}_\Omega \cdot \vec{E}_\Omega(\vec{r} - R\hat{z}) \quad (8)$$

The cosine dispersion relation of the CROW is plotted in Fig. 2.2a. The group velocity, given by the slope of the dispersion $\delta\omega/\delta k$, is expected to be drastically reduced where the dispersion is flat at the edges of the Brillouin zone ($K = 2\pi/R$), and go to zero in an ideal infinite lattice. Even for finite-length CROWs (which, obviously, are of practical interest) the band-edge mode is expected to be several orders of magnitude slower than its speed in vacuum [4].

Random variations along the lattice, however, cause the band edges to deviate from their flat shape. Disorder, important because it is

unavoidable in any fabrication process, causes the band edges do not remain flat as expected from the simplified ideal model, but instead form band "tails" (Fig 2.2b) [6, 7]. As a result, the maximum obtainable slowing factor at the band edge becomes severely limited by even a few nanometers of variation along the structure. This cannot be shown with traditional methods of band calculations including tight-binding models, plane-wave expansion, or finite-difference computational methods, because periodic boundary conditions always force the band edges to be flat [7]. Instead, accurately describing the effect of disorder requires computing the density of states $\rho(\omega)$ by solving the matrix equation [8]

$$i\frac{d}{dt}\boldsymbol{u} = M\boldsymbol{u} \tag{9}$$

where $\boldsymbol{u}$ is a column vector listing the individual resonator eigenmodes and M is a square matrix with the self and cross coupling coefficients listed as the diagonal and off-diagonal terms, respectively. Solutions of Eq. 9 are found by solving $|M - \omega I| = 0$, where I is the unit matrix. Random variations can be introduced in M without the need for periodic boundary conditions. Mathematical details are not discussed in this dissertation but can be found in ref. 8. The key consequence for slow light applications is that the slowing factor, defined [7]

$$S \equiv \frac{c}{group\ velocity\ at\ band\ edge} = \frac{\lambda}{R}\frac{1}{(\delta\kappa^2\kappa)^{1/3}} \quad (10)$$

where $\delta\kappa$ is the deviation in κ. While S is nearly infinite for an ideal structure (and infinite for an infinitely long ideal structure), just a few percent variation $\delta\kappa$ limits S to range of roughly 10-100. Thus, nearly-stopped light in a CROW, as well as any resulting nonlinearity enhancement at band edge remains elusive.

Rather than the initial goal of demonstrating slow light and nonlinearity enhancement effects, we observe a different yet interesting physically fundamental phenomenon. At or near the band edges of CROWs, disorder leads to localization of light. In this chapter we discuss the theoretical prediction and experimental observation of Anderson localization of light in weakly disordered 1D lattice. We show that unavoidable fabrication-induced variations in the structure inevitably lead to localization in all CROWs that are of sufficient length to be of interest for practical applications.

2.2 Anderson Localization of Optical Waves

Anderson localization, stated simply, is the suppression of wave transport due to random scattering in a disordered medium. Philip Anderson originally introduced this theory for electrons in solid state materials [9], and the concept was later applied to optical waves [10, 11]. Localization (of both electrons and photons) occurs in the presence of sufficient disorder such that multiple scatterings occur on length scales comparable to the wavelength; the Ioffe-Regel Criterion is met when the product of the wave vector k and the mean-free path l is less than 1 [12]. While the predicted band-edge mode wave-function is spatially extended over the entire lattice in the ideal case, localization due to random variations, defects, and disorder in the lattice causes the waves to be spatially confined (i.e., localized). Localization of photons has been experimentally observed in three-dimensional (3D) systems such as semiconductor powders [13] and 3D photonics crystals [14], in a 2D photonic lattice [15], and in 1D structures such as photonic crystal waveguides [16].

The unique feature of localization in periodic 1D structures (from 3D and 2D), and its key importance to slow light in CROWs is the inevitability that it will occur. That is, in any 1D lattice provided that is sufficiently long, localization will occur for **any** value of disorder [17]. This can be most easily

shown by considering the energy separation of the first two eigenmodes at the δE, given by

$$\delta E = 2\kappa|\cos[\pi N/(N+1)] - \cos[\pi(N-1)/(N+1)]|$$
$$\approx 3\kappa\pi^2/N^2 \quad (11)$$

where κ is the nearest-neighbor coupling coefficient and N is the number of unit cells. The energy perturbation due to disorder scales as $\delta\kappa/\sqrt{N}$. The onset of localization can be considered to be the point at which this energy perturbation exceeds the energy separation δE. Indeed, for **any** non-zero value of disorder $\delta\kappa$, there is some value of N (which we can define as threshold N_{th}) that will cause this onset of localization. For 3% disorder $N_{th} = 93$ and for 5% disorder $N_{th} = 66$. For silicon microresonators, this corresponds to only a few nanometers of disorder [6, 7] which is within the fabrication tolerance of advanced CMOS processing techniques.

Previous observations of localization [13-16] were induced by intentionally introducing disorder into the structures under investigation. Since all device fabrication processes have some tolerances, small variations introduced by the fabrication of any CROW should lead to localization in long structures. Since long structures comprising 100 or more

resonators are required for slow light applications [18], localization is expected in practical structures. Here we demonstrate localization in a CROW whose unit cells are nominally identical and only weak disorder due to fabrication imperfections are present.

2.3 Experiment

2.3.1 Device Fabrication

CROWS composed of square-block resonators (1.5 μm x 1.5 μm x 0.5 μm) periodically loading a single-mode SOI waveguide (250 nm width x 500 nm height), shown in figure 2.3, were fabricated using e-beam lithography and dry-etching techniques. SOI chips with a 500 nm silicon device layer and 1 μm buried oxide layer (BOX) were spin-coated with PMMA positive-tone resist, and the pattern exposed by e-beam lithography and developed in MIBK. A 35 nm layer of Ni metal was e-beam evaporated onto the resist surface and lifted off using acetone, leaving the Ni pattern to serve as an etch mask for reactive ion etching (RIE). The silicon was etched down to the BOX to form the waveguide structure, and the samples were immersed in nickel etchant (Transene, type TFB) to remove the Ni etch mask. The chips were then lapped to a thickness of 200 μm, cleaved to form the input and output waveguide facets, and mounted for testing.

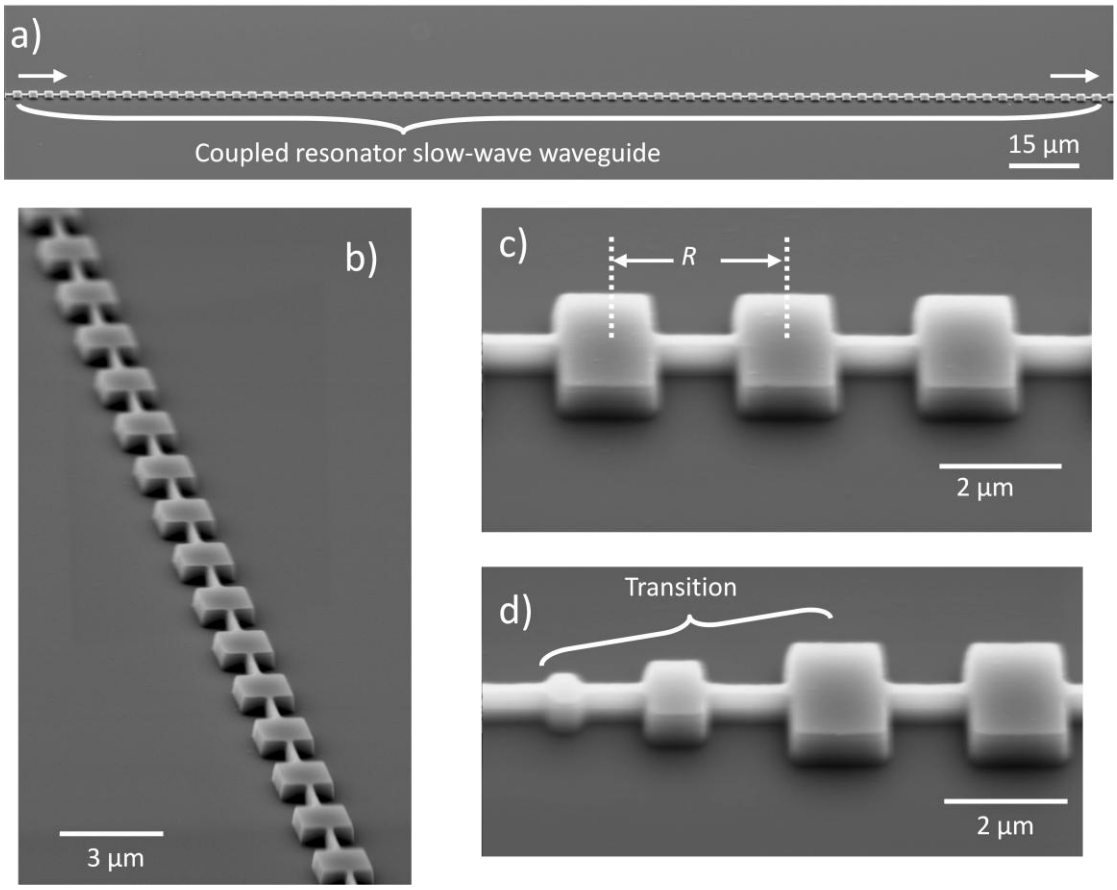

Figure 2.3: Fabricated CROW structures. a) Side and b) perspective images of the fabricated 100-resonator CROW. c) Close-up of the individual resonators showing a single unit cell. d) Input and output transition regions.

2.3.2 Measurement of Localization

Light from a tunable continuous-wave (CW) laser (Agilent 81640A) with an input power of 100 µW was coupled into the silicon chips using polarization-maintaining lens-tipped fibers (Oz-Optics), aligned to the chip using six-axis micrometer stages (Newport Ultralign) equipped with differential micrometers. The spectrum was recorded by sweeping the

laser wavelength and monitoring the output using an InGaAs photodiode while recording the wavelength.

To record the spatial distribution of the field, a modified knife-edge method was used (Fig. 2.4), a simple and robust method insensitive to misalignment, knife edge diffraction and geometric aperturing [19]. The device plane was confocally imaged using a microscope (Olympus BX series, with Mitutoyo M-Plan-APO NIR objective) focused onto a highly sensitive InGaAs photoreceiver (New Focus Femtowatt 2153) such that the field of view at the detector images the slow-wave section, and not the input/output fibers or chip facets. The laser source was set to the wavelength of interest (e.g. at or near the band edge) and was modulated at a frequency less than 750 Hz while the photoreceiver output was measured by a lock-in amplifier (Stanford Research Systems SR830). As the knife edge was scanned across the field of view at a constant speed (using a Newport ILS translation stage and ESP300 motion controller), the resultant power vs. position trace was recorded. The field profiles were obtained by smoothing the traces using a moving average filter with a window of 250 nm, which is not more than the calibrated precision of the linear stage, and differentiating the resultant trace. To factor out the coupling and background absorption features, all traces were normalized to the same 'control' trace of an extended field away

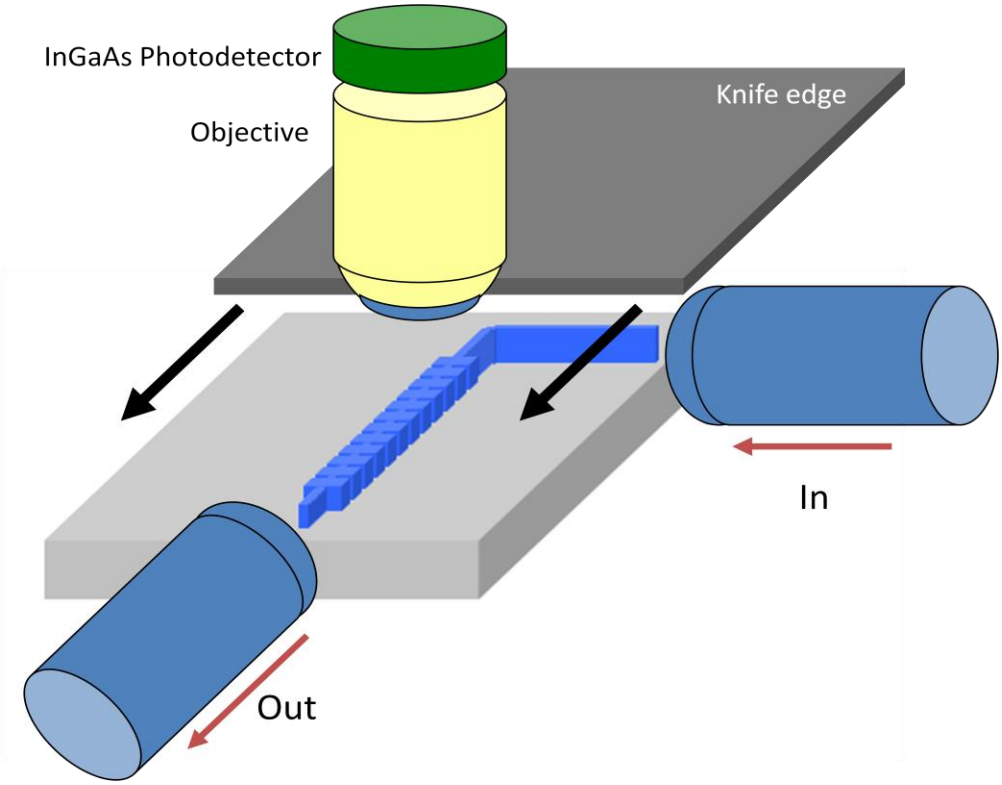

Figure 2.4: Knife-edge scan measurement of spatial field profile. With the input wavelength tuned near the band edge, a knife edge is scanned across the device while the detected power is recorded as a function of knife edge position.

from band edge. It is implicitly assumed that the coupling and background loss coefficient do not vary over the 2 nm spectral window of interest, which is substantially narrower than the narrowest bandwidth of any optical elements in the measurement set-up.

Figure 2.5 shows the measured spatial profiles. The calculated dispersion is shown in Fig. 2.5a with the measured transmission spectrum near the band edge in Fig. 2.5b. At various points near the band edge, the corresponding measured spatial field profiles are shown in Fig. 2.5c.

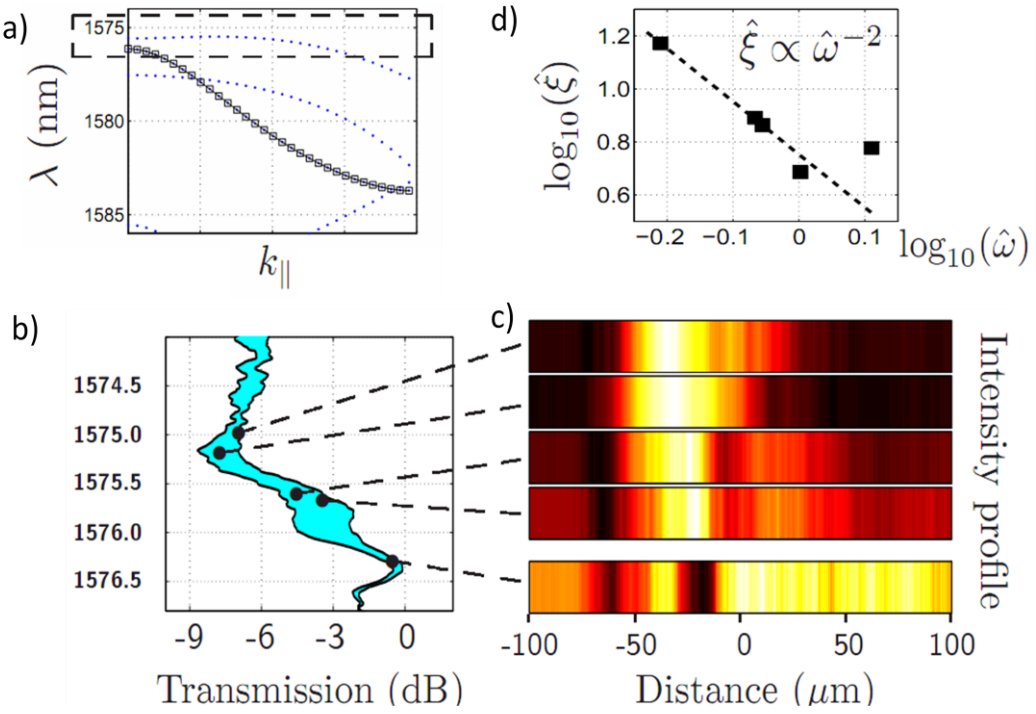

Figure 2.5: Measurement of localization. a) Calculated dispersion relation and b) measured transmission spectrum of the CROW near the band edge. c) Measured spatial field profiles show localized fields at the band edge and extended fields away from the band edge. d) Log-log plot of localization length vs. frequency (normalized units) agrees well with theory (ref. 17)

Scans at the band edge show that light is localized to a few unit cells, while scans away from the band edge show field profiles extending the entire length of the structure. This is direct observation of light localization. Fig 2.5d plots localization length as a function of normalized frequency, in good agreement with theoretical predictions [17]. Average sidewall roughness of the fabricated structures measured by atomic force microscopy (AFM) (Fig 2.6) was 10 nm with a correlation length of 75 nm, indicating reasonable fabrication tolerance with current microfabrication

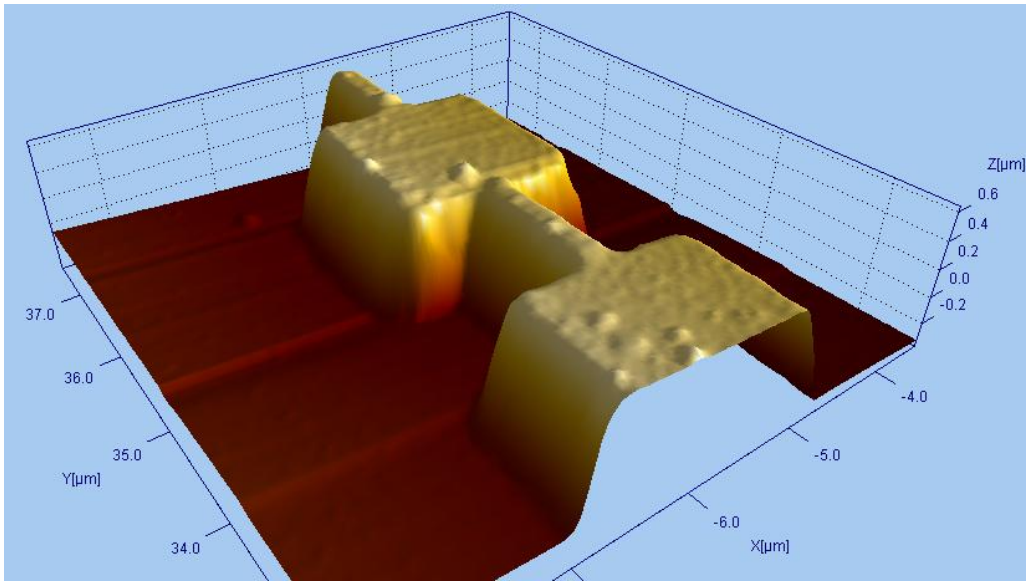

Figure 2.6: AFM measurement of sidewall roughness. Example AFM scan of the fabricated CROW structures. Tilted-sample scans of the etched sidewalls show sidewall roughness of ~10 nm with a correlation length of ~75 nm.

techniques. Hence, the observed localization was induced by inherently unavoidable disorder.

2.4 Summary and Conclusion

We have demonstrated the Anderson localization of optical waves in an optical slow wave structure. We demonstrate that localization occurs in a 1D lattice due to unavoidable disorder present in all practical fabricated structures. While slow-light is strongly limited by disorder, this may lead to a new class of devices in which localization is not only present but utilized as part of the engineered device characteristics.

REFERENCES

[1] Y. A. Vlasov, M. O'Boyle, H. F. Hamann, S. J. McNab, "Active control of slow light on a chip with photonic crystal waveguides," *Nature*, **438**, 65 (2005)

[2] J. E. Heebner, R. W. Boyd, Q. H. Park, "Slow light, induced dispersion, enhanced nonlinearity, and optical solitons in a resonator-array waveguide," *Physical Review E*, **65**, 036619 (2002)

[3] A. Melloni, F. Morichetti, C. Ferrari, M. Martinelli, "Continuously tunable 1 byte delay in coupled-resonator optical waveguides," *Optics Letters*, **33** (20), 2389 (2008)

[4] Y. Chen, S. Blair, "Nonlinearity Enhancement in Finite Coupled-Resonator Optical Waveguides," *Optics Express*, **12** (15), 3353 (2004)

[5] S. Mookherjea, "Coupled-Resonator Optical Waveguides and Multiplexed Solitons," PhD Dissertation, California Institute of Technology, 2003

[6] S. Mookherjea, A. Oh, "Effect of disorder on slow light velocity in optical slow-wave structures," *Optics Letters*, **32** (3), 289 (2007)

[7] S. Mookherjea, J. S. Park, S. H. Yang, P. R. Bandaru, "Localization in Silicon Nanophotonic Slow-Light Waveguides," *Nature Photonics*, **2** (2), 90-93 (2008)

[8] S. Mookherjea, "Spectral Characteristics of Coupled Resonators," *Journal of the Optical Society of America B*, **23**, 1137-1145 (2006)

[9] P. W. Anderson, "Absence of Diffusion in Certain Random Lattices," *Physical Review*, **109** (5), 1492-1505 (1958)

[10] P. W. Anderson, "The question of classical localization A theory of white paint?" *Philosophical Magazine B*, **52** (3), 505-509 (1985)

[11] S. John, "Electromagnetic Absorption in a Disordered Medium near a Photon Mobility Edge," *Physical Review Letters*, **53**, 2169-2172 (1984)

[12] A. F. Ioffe, A. R. Regel, *Progress in Semiconductors*, edited by A. F. Gibson (John Wiley & Sons, Inc., New York, 1960), **4**, 237

[13] D. S. Wiersma, P. Bartolini, A. Lagendijk, R. Righini, "Localization of Light in a Disordered Medium," *Nature*, **390**, 671-673 (1997)

[14] Y. A. Vlasov, M. A. Kaliteevski, V. V. Nikolaev, "Different Regimes of Light Localization in Disordered Photonic Crystal," *Physical Review B*, **60**, 1555-1562 (1999)

[15] T. Schwartz, G. Bartal, S. Fishman, M. Segev, "Transport and Anderson Localization in Disordered Two-Dimensional Photonic Lattices," *Nature*, **446**, 52-55 (2007)

[16] J. Topolancik, B. Ilic, F. Vollmer, "Experimental Observation of Strong Photon Localization in Disordered Photonic Crystal Waveguides," *Physical Review Letters,* **99**, 253901 (2007)

[17] P. Sheng, *Introduction to Wave Scattering, Localization, and Mesoscopic Phenomena*, Academic Press, San Diego, 1995

[18] F. Xia, L. Sekaric, Y. Vlasov, "Ultracompact Optical Buffers on a Silicon Chip," *Nature Photonics*, **1** (1), 65 (2007)

[19] A. H. Firester, M. E. Heller, P. Sheng, "Knife-edge scanning measurements of sub-wavelength focused light beams," *Applied Optics*, **16**, 1971 (1977)

Chapter 2 contains material published in:

- S. Mookherjea, J. S. Park, S. H. Yang, P. R. Bandaru, "Localization in Silicon Nanophotonic Slow-Light Waveguides," *Nature Photonics*, **2** (2), 90 (2008)

The dissertation author contributed experimental work to the paper. The primary author planned and supervised the research, provided theoretical work, and assisted with experimental work and data analysis.

Figure 2.1c is copyright IBM.

3. FOUR-WAVE MIXING IN SILICON WAVEGUIDES

3.1 Introduction

In this chapter we utilize the third-order nonlinearity $\chi^{(3)}$ of silicon waveguides for wavelength conversion through four-wave mixing (FWM), sometimes referred to as four-photon mixing, or simply parametric mixing. To most basically explain the origin and significance of the third-order nonlinearity, we start with the response of a medium to the electric field of an optical wave, E, propagating within the medium given by its polarizability, $P = \chi E$. The susceptibility of the medium, χ, can be expanded into its linear and nonlinear terms $\chi = \chi^{(1)} + \chi^{(2)} + \chi^{(3)} + \ldots$ [1, 2]. The second order nonlinear $\chi^{(2)}$ only occurs in non-centrosymmetric materials, which does not apply to the materials of interest in this dissertation, and we focus on nonlinear interactions arising from $\chi^{(3)}$. Two important quantities are the Kerr coefficient $n_2 = 3\chi^{(3)}/2n_0\epsilon_0 c$, and the nonlinearity coefficient $\gamma = n_2\omega_0/cA_{eff}$.

As mentioned in Chapter 1, four-wave mixing (FWM) is a parametric process in which the interaction of a pump and probe through $\chi^{(3)}$ generates an idler wave whose frequency is equal to the difference between twice the pump frequency and the probe frequency. Two pump

photons give their energy to create one photon at each the probe frequency and idler frequency. As a result, the pump converts, or copies, the signal to the idler wavelength. This interaction is described by the coupled-mode equations [2]

$$\frac{\partial}{\partial z}A_{p1} + \frac{1}{2}\alpha_{p1}A_{p1} = i\gamma_{p1}\left[\left|A_{p1}\right|^2 + 2\left|A_{p2}\right|^2 + 2|A_s|^2 + 2|A_i|^2\right]A_{p1} + 2i\gamma_{p1}A_s^*A_{p2}A_i e^{(i\Delta\beta z)} \quad (3.1)$$

$$\frac{\partial}{\partial z}A_{p2} + \frac{1}{2}\alpha_{p2}A_{p2} = i\gamma_{p2}\left[\left|A_{p2}\right|^2 + 2\left|A_{p1}\right|^2 + 2|A_s|^2 + 2|A_i|^2\right]A_{p2} + 2i\gamma_{p2}A_{p1}A_sA_i^* e^{(-i\Delta\beta z)} \quad (3.2)$$

$$\frac{\partial}{\partial z}A_s + \frac{1}{2}\alpha_s A_s = i\gamma_s\left[|A_s|^2 + 2\left|A_{p1}\right|^2 + 2\left|A_{p2}\right|^2 + 2|A_i|^2\right]A_s + 2i\gamma_s A_{p1}^*A_{p2}A_i e^{(i\Delta\beta z)} \quad (3.3)$$

$$\frac{\partial}{\partial z}A_i + \frac{1}{2}\alpha_i A_i = i\gamma_i\left[|A_i|^2 + 2\left|A_{p1}\right|^2 + 2\left|A_{p2}\right|^2 + 2|A_s|^2\right]A_0 + 2i\gamma_i A_{p1}A_{p2}^*A_i e^{(-i\Delta\beta z)} \quad (3.4)$$

where A_n $(n = p1, p2, s, i)$ is the field amplitudes of the pumps, signal, and idler, respectively, and α_n and γ_n are the corresponding propagation loss and nonlinear coefficients. The phase mismatch is given by

$$\Delta\beta = \beta_i - \left[\beta_s + \left(\beta_{p1} - \beta_{p2}\right)\right], \quad (3.5)$$

which can also be expressed in terms of the respective wave vectors k using the relation $\beta = kn_{eff}$. In degenerate (single-pump) FWM, the pump photons $p1$ and $p2$ are provided by a single pump wave.

Conversion efficiency is defined as the ratio of the generated idler power to the input signal power,

$$G = \frac{P_{i,out}}{P_{s,in}} = \left[\gamma \frac{P_p}{g} \sinh(gL)\right]^2 \quad (3.6)$$

where the gain parameter g is given by

$$g = \left[\gamma P_p \Delta k - (\Delta k/2)^2\right]^{1/2}. \quad (3.7)$$

Parametric gain is achieved if the input signal power is amplified, while net conversion efficiency (or conversion gain) occurs if the output idler power exceeds the input signal power.

As discussed previously, FWM has many applications to signal processing for communications applications and light generation and amplification. In this chapter we discuss the fundamental aspects of the FWM process, from the optimization of SOI waveguide design and

fabrication processing, to experimentally measuring FWM in silicon waveguides.

3.2 Waveguide Design

3.2.1 Group Velocity Dispersion

FWM is a coherent process, and efficient conversion requires phase matching. Both the energy and momentum of the photons involved in the process must be conserved. In other words, photons generated from the FWM process at different spatial points along the waveguide must add up in phase. Phase matching in guided-wave devices such as optical fiber and waveguides consists of minimizing the group velocity dispersion (GVD). This is commonly quantified by the dispersion parameter D, defined as

$$D = \frac{d}{d\lambda}\beta_1 = 1\left(\frac{2\pi c}{\lambda^2}\right)\beta_2 = -\left(\frac{\lambda}{c}\right)\frac{d^2}{d\lambda^2}n_{eff} \tag{3.8}$$

generally defined in units of ps/(nm.km), where λ is the free-space wavelength, c is the speed of light, n_{eff} is the modal effective index of the

waveguide (or fiber) as a function of wavelength. The quantities β_1 and β_2 are taken from the expansion of the propagation constant β

$$\beta = \frac{\omega}{c} n(\omega) = \beta_0 + \beta_1(\omega - \omega_0) + \frac{1}{2}\beta_2(\omega - \omega_0)^2 + \ldots \quad (3.9)$$

where

$$\beta_1 = \frac{1}{c}\left(n_{eff} + \omega \frac{\partial n_{eff}}{\partial \omega}\right) = {}^{1}/_{v_g} \quad (3.10)$$

and

$$\beta_2 = \frac{1}{c}\left(2\frac{\partial n_{eff}}{\partial \omega} + \omega \frac{\partial^2 n_{eff}}{\partial \omega^2}\right) \quad (3.11)$$

where v_g is the group velocity and ω is the angular frequency of light. The overall dispersion of a waveguide is the combination of material dispersion (the dependence of the material dielectric constant on frequency) and waveguide dispersion (the dependence of the modal propagation constant with frequency). Since the material dispersion of

silicon is fixed, GVD is minimized when waveguide dispersion is tuned cancel the material dispersion. Here we explore two simple approaches of tuning waveguide dispersion: by adjusting the waveguide cross-sectional dimensions, and by adding a conformal thin-film cladding.

3.2.2 Waveguide Dispersion Tuning

The simplest way to tune waveguide dispersion is to adjust the cross-sectional dimensions of the waveguide. For a given waveguide height (which is most generally fixed by the SOI wafer device layer thickness), the simplest approach is to fabricate the waveguide with a particular designed width. Figure 3.1 plots the dispersion parameter D [ps/nm.km] with wavelength for SOI waveguides with 250 nm height and various widths. From these dispersion curves, we can select the appropriate waveguide width for zero-GVD at 1550 nm.

In cases where large cross-sectional waveguide dimensions are required to minimize GVD, the increased modal effective area A_{eff} may result in a reduced nonlinear coefficient γ. An alternative approach is to use waveguides of smaller cross-sectional areas and to tune the dispersion with a conformal thin-film cladding grown after the waveguide has been formed [6]. A cross section of such a structure is shown in Fig 3.2. After the

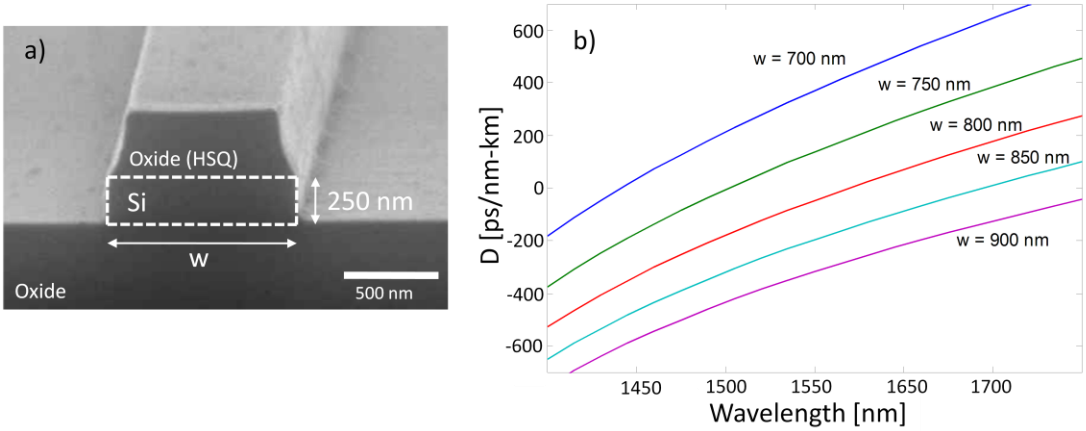

Figure 3.1: Silicon waveguide dispersion curves. a) Cross section of a typical SOI waveguide with a height of 250 nm and a 250 nm thick HSQ layer retained after fabrication. b) Group velocity dispersion curves for the corresponding waveguides as a function of waveguide width.

silicon-etch process during waveguide fabrication, and before the input and output polymer overlay regions are formed, a thin film of silicon nitride (SiN) is grown using plasma-enhanced chemical vapor deposition (PECVD). The waveguide dispersion is strongly dependent on the thickness of the SiN thin film cladding, as illustrated in Fig 3.2.

The primary advantage to this technique is that the modal effective area A_{eff} is smaller than typical silicon waveguides designed for zero dispersion near 1550 nm [6]. However, an important trade off is that silicon free carrier lifetime is significantly increased by the SiN surface passivation [7], leading to increased free-carrier loss. We present FWM measured in waveguides with dispersion engineered using both of these techniques.

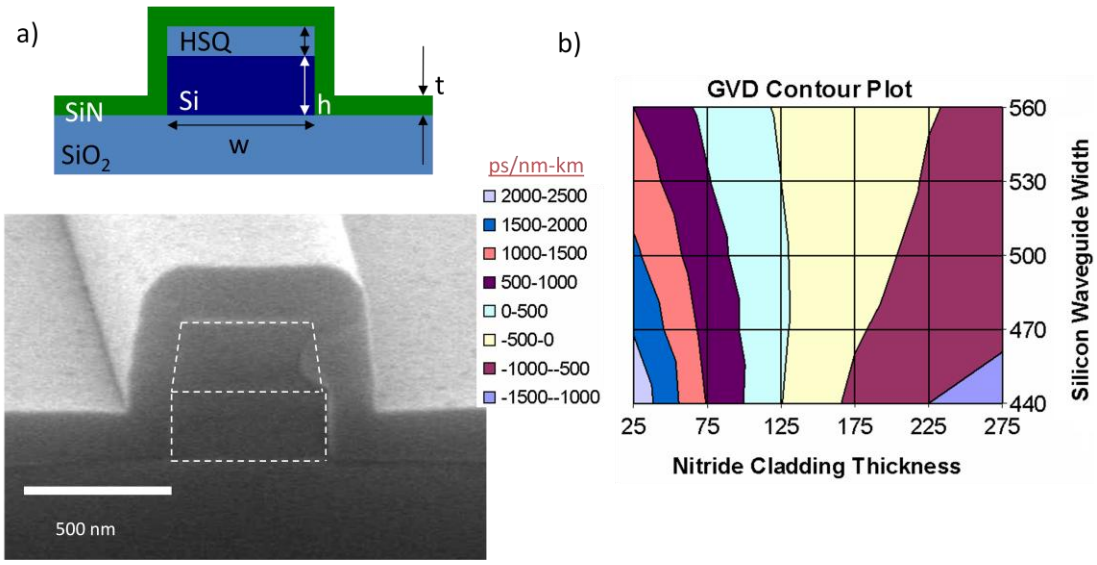

Figure 3.2: Silicon waveguide dispersion curves with SiN cladding. a) Cross section of an SOI waveguide with a SiN thin-film cladding. b) Group velocity dispersion contour plots for the corresponding waveguides as a function of waveguide width and nitride thickness.

3.2.3 Inverse Taper Chip-to-Fiber Coupler

Using off-chip sources, waveguides with low coupling loss to input and output fibers as well as low propagation loss are crucial for FWM experiments, as they are highly power-dependent. Due to the large mismatch in size of the 2.5 μm spot size of the input and output lens-tipped fibers to the much smaller modal area of the silicon waveguides, efficient coupling into and out of the silicon chip requires careful engineering of the couplers. Efficient coupling was achieved by use of silicon inverse tapers overlaid with SU-8 polymer waveguides (Figure 3.3) [3-5]. The silicon

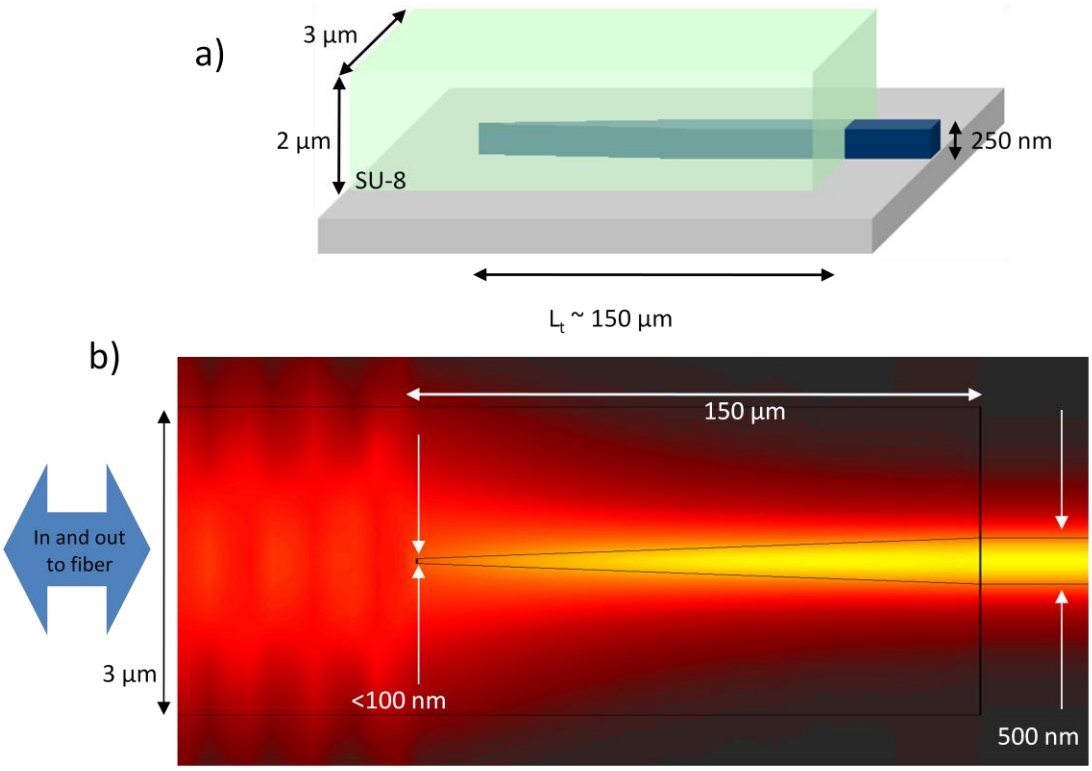

Figure 3.3: Inverse taper couplers. a) Schematic of the silicon inverse taper overlayed with a polymer waveguide cladding. b) Two-dimensional BPM simulation shows field becoming delocalized from the waveguide core as the taper narrows, providing efficient coupling to the larger polymer waveguide mode.

waveguide width was tapered own to a point as small as possible, limited by lithography resolution, which for our experiments was generally 30 to 70 nanometers. Polymer waveguides with 1-2 µm height and 3-5 µm width were laid over this tapered region. The cross-sectional area of the mode traveling along the taper increased along the taper as the silicon waveguide width decreased, matching to the large modal area of the polymer waveguide. The large modal area of the polymer waveguide provided much better match to the lensed fibers, providing efficient

overall coupling efficiency from the fiber to the silicon waveguide. The most efficient couplers demonstrated in our experiments provided 8 dB input to output fiber-to-fiber insertion loss.

3.3 Device Fabrication

In contrast to the work in Chapter 2, a fabrication process that avoided the use of metallic etch masks was required to avoid metallic contamination during etching, which tends to results in extraneous optical loss [10]. Instead, Hydrogen silsesquioxane (HSQ) was used, also known as FOX flowable oxide (Dow Corning). This e-beam-sensitive spin-able glass served as both a negative-tone e-beam lithography resist and a hard mask for silicon dry etching.

The process started with SOI wafers (SOITEC) with 250 nm device silicon layer with [110] surface crystal orientation sitting on a 3μm buried oxide (BOX) layer, and a 700 μm silicon handle substrate. Before processing the wafers were diced into individual chips by the UCSD Nano3 staff, with anywhere from 0.5 to 1 μm PMMA layer coated to protect the silicon surface. The chips were solvent-cleaned using ultra-sonic at low power in acetone for 10 minutes, isopropanol for 5 minutes, and de-ionized (DI) water for 1 minute. The standard "RCA clean" was also used at times, consisting of an organic clean in a 5:1:1 DI

water/hydrogen peroxide/ammonium hydroxide mixture at 70°C, a short buffered-HF oxide strip, and a inorganic clean in a 6:1:1 DI water/hydrogen peroxide/hydrochloric acid mixture again at 70°C. Though this is the most thorough silicon cleaning technique, the solvent clean was found to be sufficient for new SOI samples and was used on the vast majority of samples processed for this work.

The cleaned samples were immediately spin-coated with FOX resist for e-beam lithography patterning. Because of the sensitivity of the FOX film to any minute particles on the silicon surface, the solvent cleaning of the samples and FOX coating were done in continuous steps in a class 100 area located in the e-beam lithography lab of the Nano3 cleanroom. FOX13 was spin coated onto the silicon samples at 1500 rpm for 60 seconds at a low acceleration, then soft-baked at 150°C for 5 minutes on a level hotplate. The resulting HSQ films were 220-250 nm in thickness.

Patterning by e-beam lithography was performed using two separate systems: a Raith50 system located in Nano3 at UCSD, and a Leica EBPG5000+ located at the University of Central Florida. The Raith50 was equipped with a 30 kV column while the Leica was equipped with a 100 kV column. Patterning of FOX13 with the Raith50 required an e-beam dosage of 1000-1500 $\mu C/cm^2$, and had a maximum field of view of 600 x 600 μm^2. Although the Raith50 is capable patterning with smaller write

fields and stitching (moving the sample stage incrementally by a single write field size to pattern an area covering several write fields), stitching errors of 20-50 nm were observed in test patterns, causing excessive waveguide scattering loss. Patterning using the Leica system required a dosage of 2000-5250 μC/cm^2 (depending on feature size, due to proximity effect) with the higher dosage compared to the Raith50 due to the higher column acceleration voltage. The write field size was 160 μm, and waveguides over 6 mm in length were fabricated, representing continuous patterning over 40 write fields with very low stitching error which in most cases were too small to measure by scanning electron microscopy (SEM). Although waveguides with inverse tapers patterned by Raith50 were measured with low chip-to-fiber coupling loss (~13 dB fiber-to-fiber loss), it was determined through several test patterns that the Leica system consistently produced more accurate patterns with higher resolution over a larger write area, and ultimately waveguides with lower coupling and propagation loss.

After patterning, the FOX resist was developed by immersing in tetramethylammonium hydroxide (TMAH) with minimal slow agitation for one minute and rinsing in de-ionized water. The resulting negative-tone resist pattern served as a hard mask for silicon etching. An Oxford silicon etcher was used for the inductively-coupled plasma reactive ion etching

(ICP-RIE) process, using a combination of C_4F_8 (46 sccm) and SF_6 (25 sccm) at 15 milli-Torr pressure at 15°C using an RF power of 30 W and inductive power of 1200 W. The gas flow ratio and plasma was optimized to produce straight, vertical etch profiles with minimal roughness. The etch process was optimized such that the dominant source of waveguide sidewall roughness was that which was transferred from the etch mask, evident by straight, vertical stripes on the etched sidewalls (Fig 3.4b, c). Post-processing to reduce sidewall roughness by silicon oxidation was not explored in this work due to unavailability of silicon oxidation furnaces, but may further improve sidewall roughness.

After dry-etching the silicon down to the BOX to form the waveguide structure, the input and output inverse-tapered regions were overlaid with polymer waveguides by photolithography. The samples were spin-coated with SU-8 2002 (Microchem) at 1500 rpm for 1 minute, then soft-baked on a level hotplate at 90° C for 1 minute. A photolithography mask with 1 mm long and 3 μm wide waveguide patterns were aligned to the sample using a Karl Suss MA6 mask aligner and exposed with a 7.5 mW/cm^2 intensity UV lamp for 20 seconds. The exposed resist was then post-exposure-baked at 90° C for 10 seconds, then developed in SU-8

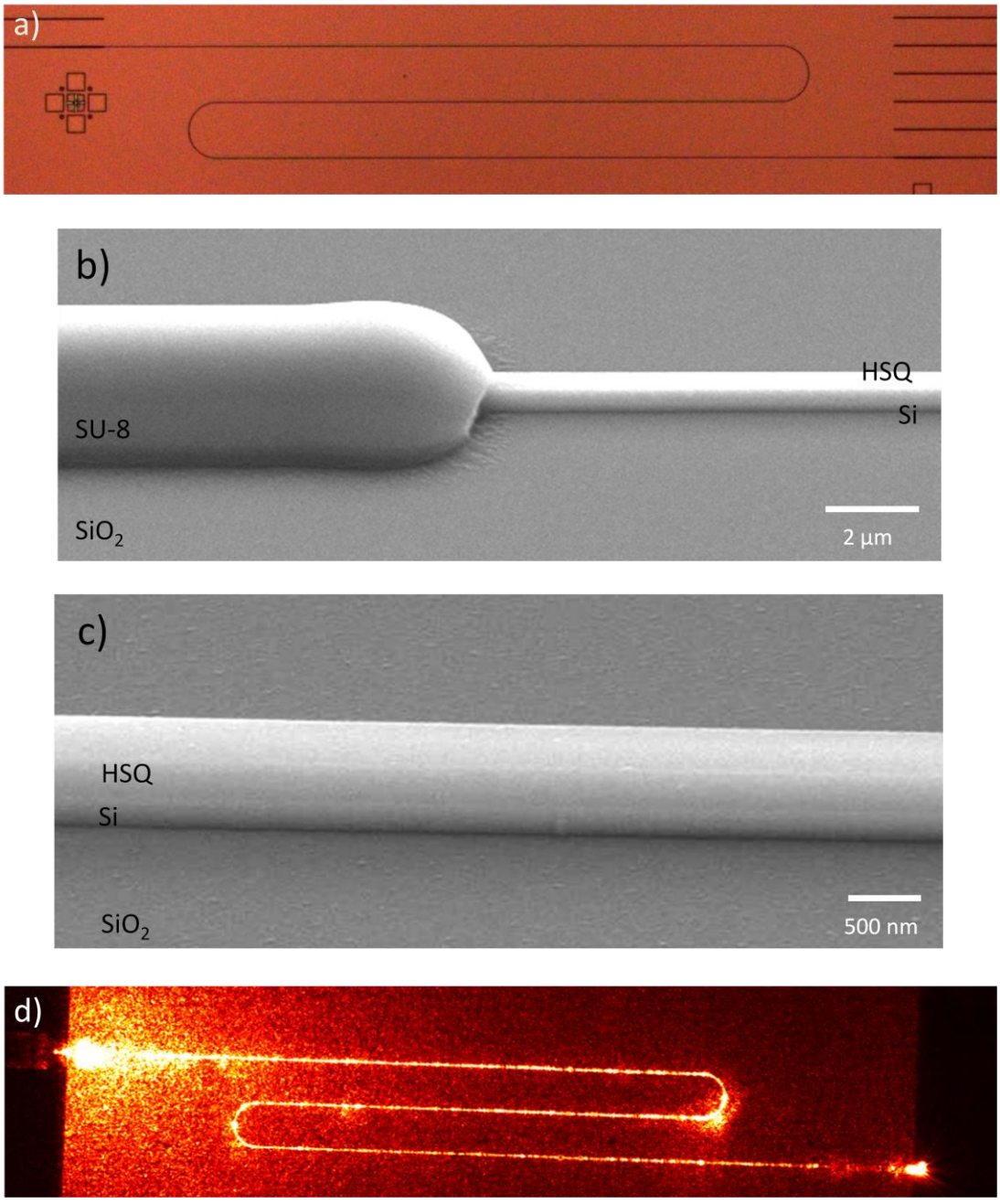

Figure 3.4: Fabricated waveguides structures. a) Optical microscope image of a 5.9 mm long waveguide. b) Polymer coupler overlaying the silicon waveguide and c) waveguide angled images show good quality waveguide sidewalls. d) Infrared image of 1550 nm light coupled into and out of the waveguide shows minimal scattering due to lithography stitching error and fabrication imperfections.

developer (Microchem). The resulting SU-8 patterns were then hard baked at 150° C for at least 15 minutes (and in most cases longer). Silicon nitride thin film claddings described in section 3.2.2 were produced by plasma-enhanced chemical vapor deposition (PECVD) of the SiN material using an Oxford Plasmalab PECVD system on the waveguides before polymer overlay.

Waveguides up to 5.9 mm in length, not including the input and output inverse-tapered regions, were produced. Propagation loss was measured by cut-back method to be 2.8 dB/cm. The waveguides used for FWM measurements were 3.8 mm in length and had fiber-to-fiber coupling efficiency up to -8 dB. Figure 3.4 shows optical microscopy and scanning electron microscopy (SEM) images of fabricated waveguides.

3.4 Four-Wave Mixing Measurements

3.4.1 Experimental Setup

The experimental setup for FWM measurements is shown in figure 3.5. The pump was produced from a tunable external cavity laser (ECL) was amplitude modulated using a lithium niobate modulator to produce 100 picosecond pulses with a 1 or 10 MHz repetition rate. The 100 ps pulse duration is selected such that nonlinear absorption is not avoided [8, 9] in

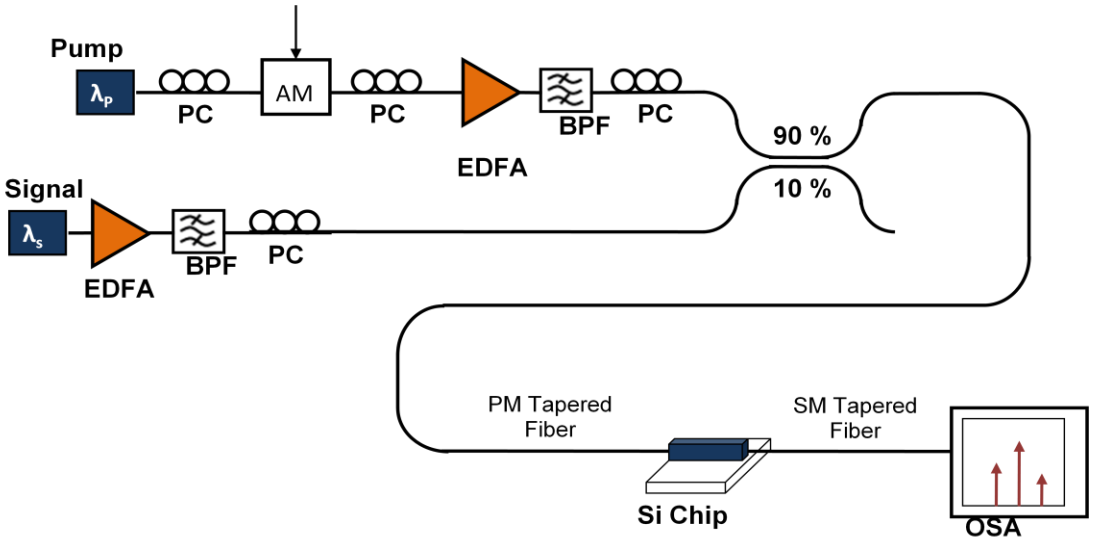

Figure 3.5: FWM measurement setup. Schematic of the measurement setup used for the FWM measurements. Abbreviations: PC: polarization controller, AM: amplitude modulator, EDFA: erbium-doped fiber amplifier, BPF: band-pass filter, OSA: optical spectrum analyzer

order to gain insight into continuous-wave (CW) performance, yet allows reasonable peak power to be generated from the erbium-doped fiber amplifiers (EDFA) used in our experiments. The pump was then amplified using a C-band EDFA and band-pass filtered to remove amplified spontaneous emission (ASE) noise. The CW probe signal was produced from a tunable laser also amplified by an EDFA and band-pass filtered. The pump and signal were combined using a 90/10 coupler, and coupled into the silicon chip using lens-tipped fibers. The peak power of the pulsed pump was 31 dBm, and the power of the CW signal was 4 dBm. The input and output couplers were reciprocal, confirmed by simulation using RSOFT BeamProp simulation tool. Consequently, the peak pump power inside

the waveguide is estimated to be 624 mW. The output of the silicon chip was fiber-coupled and observed on an optical spectrum analyzer (OSA).

3.4.2 Experimental Results

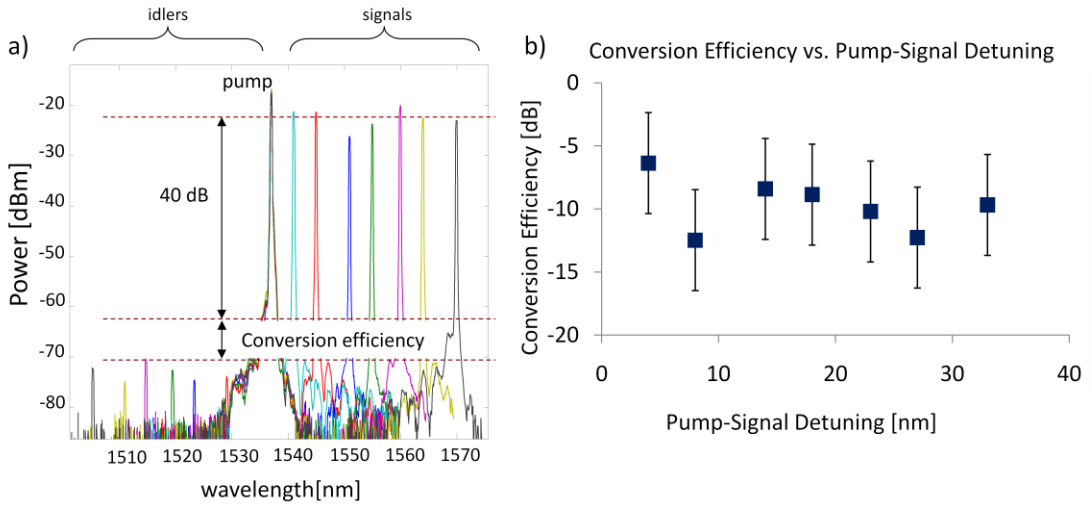

Figure 3.6: Degenerate FWM measurement results. a) FWM spectra recording for the pump tuned to 1537 nm and the signal tuned through the C band. b) Conversion efficiency plotted as a function of pump-signal wavelength detuning.

The FWM results are shown in figure 3.6. Figure 3.6a shows FWM conversion from a waveguide with 550 nm x 250 nm cross sectional dimensions and 5.9 mm in length, with the pump at 1537 nm and signal tuned from 1540 nm to 1570 nm. Conversion efficiency is plotted as a function of pump-signal detuning in figure 3.6b, showing flat conversion across the measured range spanning the C band. The 4 dB error bars are calculated from 2 dB pump power variation in the various measurements

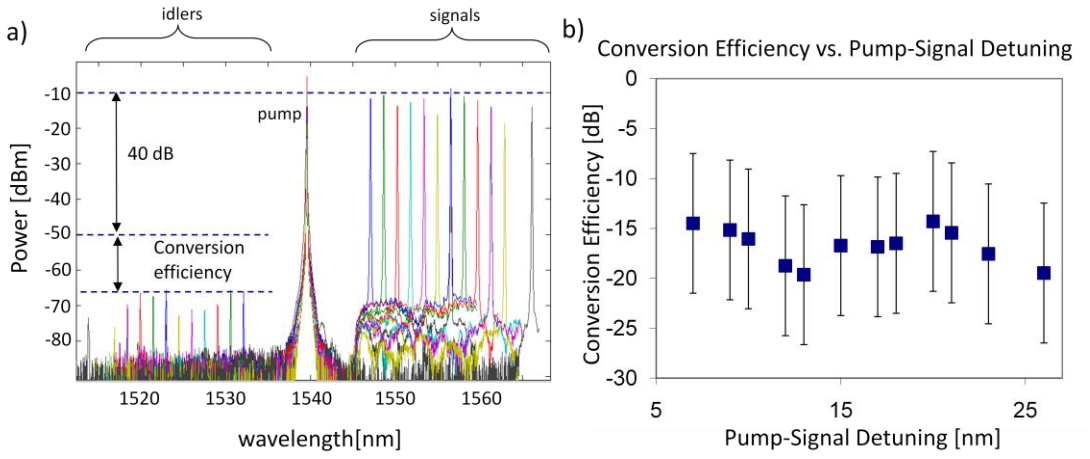

Figure 3.7: FWM measurement results with SiN cladding. a) FWM spectra measured for a waveguide with a 156 nm thick SiN thin-film cladding. b) Conversion efficiency plotted as a function of pump-signal wavelength detuning.

due to drift in fiber alignment.

Figure 3.7 shows the result obtained from a silicon waveguide with the same cross sectional area and total length, but with a 156 nm thick SiN thin film cladding. Conversion efficiency vs. pump-signal wavelength detuning, plotted Fig. 3.7b, shows flat conversion over the measured range but lower overall conversion efficiency in comparison to those obtained from waveguides without cladding. As mentioned in 3.2.2, the lower conversion is primarily attributed to higher free-carrier-induced losses due to an increase in free carrier lifetime from the SiN surface passivation.

The maximum conversion efficiency of -5.7 dB was measured from a straight waveguide with 800 nm x 250 nm in cross sectional dimensions and 3.8 mm in length, with the pump tuned to 1547 nm (figure 3.8). In

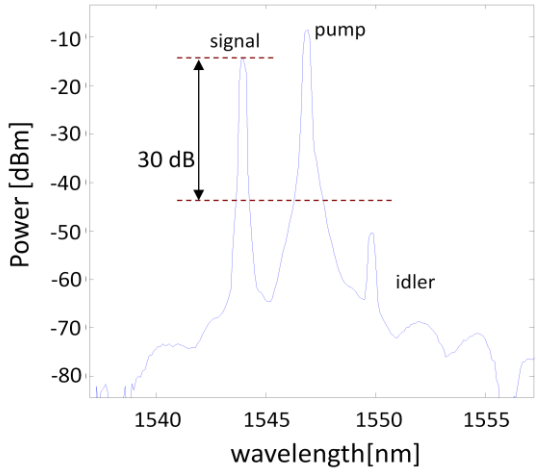

Figure 3.8: Highest achieved FWM conversion. FWM spectrum showing the maximum achieved FWM conversion efficiency of -5.7 dB.

Table 3.1: Comparison of FWM results. Reported FWM conversion efficiency in literature compared to the result obtained here.

Report	Waveguide W x H (nm x nm)	Conversion Efficiency	Notes
Columbia/IBM – [11]	220 x 445	-21 dB	CW
NTT –[12]	200 x 400 w/ SiO_yN_x cladding	-35 dB	CW
Intel – [13]	1550 x 1500 rib with 700 nm etch depth	-8.68 dB	CW, Reverse-bias p-i-n
Intel – [14]	600 x 340, 130 nm etch depth	-5.5 dB	CW
Cornell – [9]	300 x 550 to 300 x 600	+5.2 dB	3.5 ps pump (2-12 W peak)
Cornell – [15]	300 x 500 to 300 x 750	-12 dB	CW
This work	**250 x 750**	**-5.7 dB**	**100 ps pump pulses (~570 mW peak)**

comparison to other reported results (Table 3.1) shows comparable efficiencies to those achieved with CW pumps.

3.5 Summary and Conclusion

We have demonstrated degenerate FWM in silicon waveguides. Waveguide fabrication was optimized to give low insertion loss, while two different approaches to tuning waveguide dispersion were explored. We measured FWM conversion efficiency up to -5.7 dB, consistent with previous reports in literature.

REFERENCES

[1] R. Boyd, *Nonlinear Optics*, 3rd Ed, Academic Press, Burlington, MA, 2008

[2] G. P. Agrawal, *Nonlinear Fiber Optics*, 4th Ed, Academic Press, Burlington, MA, 2007

[3] S. J. McNab, N. Moll, Y. A. Vlasov, "Ultra-low loss photonic integrated circuit with membrane-type photonic crystal waveguides," *Optics Express*, **11** (22), 2927 (2003)

[4] G. Roelkens, P. Dumon, W. Bogaerts, D. V. Thourhout, R. Baets, "Efficient silicon-on-insulator fiber coupler fabricated using 248-nm-deep UV lithography," *IEEE Photonics Technology Letters*, **17** (12), 2613 (2005)

[5] T. Shoji, T. Tsuchizawa, T. Watanabe, K. Yamada, H. Morita, "Low loss mode size converter from 0.3 μm square Si wire waveguides to singlemode fibres," *Electronics Letters*, **38** (25), 1669 (2002)

[6] X. Liu, W. M. J. Green, X. Chen, I.-W. Hsieh, J. I. Dadap, Y. A. Vlasov, R. M Osgood, "Conformal dielectric overlayers for engineering dispersion and effective nonlinearity of silicon nanophotonic wires," *Optics Letters*, **33** (24), 2889 (2008)

[7] J. V. Campenhout, W. M. J. Green, X. Liu, S. Assefa, R. M. Osgood, Y. A. Vlasov, "Silicon-nitride surface passivation of of submicrometer silicon waveguides for low-power optical switches," *Optics Letters*, **34** (10), 1534 (2009)

[8] O. Boyraz, B. Jalali, "Demonstration of a silicon Raman laser," *Optics Express*, **12** (21), 5269 (2004)

[9] M. A. Foster, A. C. Turner, J. E. Sharping, B. S. Schmidt, M. Lipson, A. L. Gaeta, "Broad-band optical parametric gain on a silicon photonic chip," *Nature*, **440**, 960 (2006)

[10] T. Barwicz, C. W. Holzwarth, P. T. Rakich, M. A. Popović, E. P. Ippen, H. I. Smith, "Optical loss in silicon waveguides induced by metallic contamination," *Applied Physics Letters*, **92**, 131108 (2008)

[11] R. L. Espinola, J. I. Dadap, R. M. Osgood, S. J. McNab, Y. A. Vlasov, "C-band wavelength conversion in silicon photonic wire waveguides," *Optics Express*, **13** (11), 4341 (2005)

[12] H. Fukuda, K. Yamada, T. Shoji, M. Takahashi, T. Tsuchizawa, T. Watanabe, J. Takahashi, S. Itabashi, "Four-wave mixing in silicon wire waveguides," *Optics Express*, **31** (12), 4629 (2005)

[13] Y. H. Kuo, H. Rong, V. Sih, S. Xu, M. Paniccia, O. Cohen, "Demonstration of wavelength conversion at 40 Gb/s data rate in silicon waveguides," *Optics Express*, **14** (24), 11721 (2006)

[14] W. Mathlouthi, H. Rong, M. Paniccia, "Characterization of efficient wavelength conversion by four-wave mixing in sub-micron silicon waveguides," *Optics Express*, **16** (21), 16735 (2008)

[15] M. A. Foster, A. C. Turner, R. Salem, M. Lipson, and A. L. Gaeta, "Broad-band continuous-wave parametric wavelength conversion in silicon nanowaveguides," *Optics Express*, **15** (20), 12949 (2007)

Chapter 3 contains, in part, material presented at:

- J. S. Park, S. Zlatanovic, M. L. Cooper, J. M. Chavez-Boggio, I. B. Divliansky, N. Alic, S. Mookherjea, S. Radic, "Two-Pump Four-Wave Mixing in Silicon Waveguides," *Frontiers in Optics: OSA 93rd Annual Meeting*, FML2, San Jose, 2009

The dissertation author was the primary author of the paper.

4. DUAL-PUMP FOUR-WAVE MIXING IN SILICON WAVEGUIDES

4.1 Introduction

Parametric nonlinear devices based on four-wave mixing (FWM), as described in chapter 1, have enabled a wide range of all-optical signal processing capabilities including parametric amplification [1] time-to-frequency domain compression and manipulation, [2, 3] and ultra-high data rate multicasting and sampling [4, 5]. FWM with two (or more) pumps provides additionally degrees of freedom, leading to functionalities not otherwise achievable with a single pump. For example, in fiber-optic parametric amplifiers (FOPA), the use of two pumps enables a flat conversion spectrum with high gain over a large spectral range [6]. Additionally, ultra-high speed digital sampling benefits from multicasting through four-wave mixing (FWM) with dual pumps to produce multiple sidebands, enabling data rates otherwise not achievable with a single sampling gate [7, 8]. In contrast to fiber devices, dual pumps are not required to achieve nearly arbitrarily wide parametric conversion in silicon waveguides [9]. However, two-pump FWM may still be useful for applications in which multiple sideband generation is of interest, such as multicasting, which has already been demonstrated using a single pump on a silicon chip [10]. Thus, we characterize two-pump FWM in silicon-on-

insulator (SOI) waveguides. We demonstrate that two pumps can self-seed higher order pumps, which then produce up to nine idlers from a single signal. We also show a trade-off in maximum conversion efficiency due to nondegenerate two-photon absorption (TPA) that occurs when using two pumps in silicon.

4.2 Dual-Pump Four-Wave Mixing

4.2.1 Description of Two-Pump Four-Wave Mixing Process

FWM most commonly involves mixing of one pump with a signal and idler, where two pump photons produce one signal photon and one idler photon. FWM can also be driven by two pumps where one photon from each pump combines to produce a signal and an idler photon [11, 12]. This is illustrated in figure 4.1. Two pumps with powers P_1 and P_2 at frequencies ω_1 and ω_2 (or equivalently λ_1 and λ_2) are placed symmetrically around the zero-dispersion wavelength λ_0. A signal (probe) placed at wavelength ω_{1-} near ω_1 (where $\omega_{1-} - \omega_1 \equiv \Delta\omega$) will interact will both pumps to produce three idlers through three processes: Modulation Instability (MI), produces an idler at ω_{1-} such that $\omega_{1+} = \omega_1 + \Delta\omega$, Bragg Scattering (BS) produces an idler at ω_{2-} such that $\omega_{2-} = \omega_2 - \Delta\omega$, and Phase Conjugation (PC) produces an idler at ω_{2+} such that

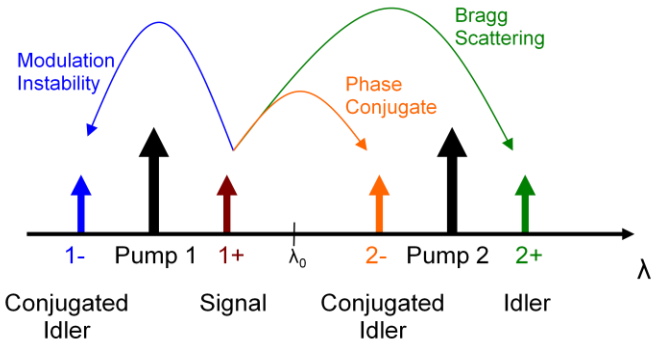

Figure 4.1: Dual-pump FWM process. Two pump parametric mixing illustrated in wavelength showing the multiple interactions that produce four sidebands: modulation instability, phase conjugation, and Bragg scattering.

$\omega_{2+} = \omega_2 + \Delta\omega$. The coupled-mode equations that describe these processes are as follows [11, 12]:

$$\frac{\partial}{\partial z}B_{1-}^{*} = -i(\delta\beta_{1-} + \gamma P1)B_{1-}^{*} - i\gamma P_1 B_{1+} - 2i\gamma\sqrt{P_1P_2}B_{2-}^{*} - 2i\gamma\sqrt{P_1P_2}B_{2+} \quad (4.1)$$

$$\frac{\partial}{\partial z}B_{1+} = i\gamma P_1 B_{1-}^{*} + i(\delta\beta_1 + \gamma P_1)B_{1+} + 2i\gamma\sqrt{P_1P_2}B_{2-}^{*} + 2i\gamma\sqrt{P_1P_2}B_{2+} \quad (4.2)$$

$$\frac{\partial}{\partial z}B_{2-}^{*} = -2i\gamma\sqrt{P_1P_2}B_{1-}^{*} - 2i\gamma\sqrt{P_1P_2}B_{1+} - i(\delta\beta_{2-} + \gamma P1)B_{2-}^{*} - i\gamma P_1 B_{2+} \quad (4.3)$$

$$\frac{\partial}{\partial z}B_{2+} = 2i\gamma\sqrt{P_1P_2}B_{1-}^{*} + 2i\gamma\sqrt{P_1P_2}B_{1+} + i\gamma P_1 B_{2+}^{*} + i(\delta\beta_{2-} + \gamma P1)B_{2+} \quad (4.4)$$

where $B_{i\pm}$ $(i = 1,2)$ are the sideband (idler or signal) amplitudes and γ is the nonlinearity coefficient defined in Chapter 3. Each sideband has a phase mismatch, given by

$$\Delta\beta_{i\pm} = \beta(\omega_{i\pm}) - \beta(\omega_i), \quad i = 1, 2. \tag{4.5}$$

The calculated gain spectrum for a two-pump parametric amplifier is shown in Fig. 4.2. An equalized response is expected between pumps over a broad spectra range, a key feature of two-pump FWM.

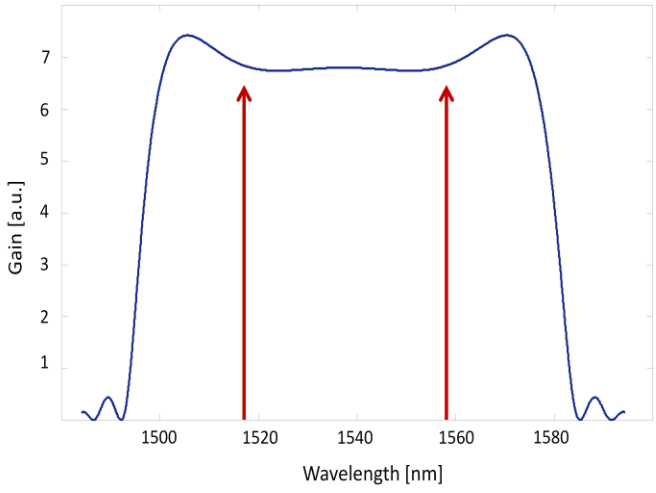

Figure 4.2: Calculated two-pump FWM spectrum. Solutions to expressions 4.1-4.4 show a broad, flat conversion spectrum with appropriately selected pump wavelengths. Nonlinear absorption is not included in the calculation.

4.2.2 Experiment

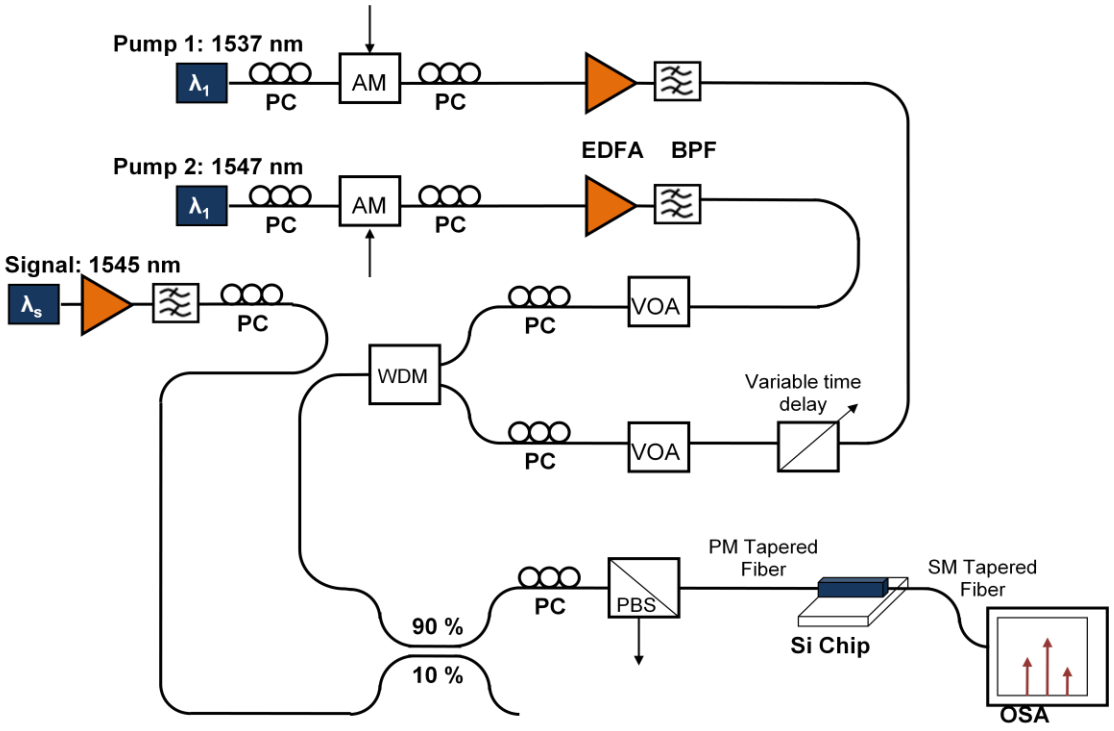

Figure 4.3: Dual FWM measurement setup. Schematic of the measurement setup used for the two-pump FWM measurements. Abbreviations: PC: polarization controller, AM: amplitude modulator, EDFA: erbium-doped fiber amplifier, BPF: band-pass filter, OSA: optical spectrum analyzer, VOA: variable optical attenuator, PBS; polarizing beam spliter

The waveguides used in our experiments were fabricated as described in Chapter 3. The cross-sectional dimensions of the waveguides used were 850 nm width x 250 nm height and 3.8 mm in length. Group velocity dispersion is plotted for different waveguide widths in Chapter 3 Fig 3.1. The total fiber-to-fiber insertion loss was 8 dB. The measurement setup is shown in Fig 4.3. Two independent pump lasers P1 and P2 (at 1547nm and 1537nm) were amplitude modulated to produce 100 ps long pulses with 10MHz repetition rate (Fig. 1). As mentioned in Chapter 3, the

100 ps pulse duration is selected such that nonlinear absorption through free-carrier absorption is not avoided [1, 13] in order to gain insight into continuous-wave (CW) performance, yet allows reasonable peak power to be generated from the erbium-doped fiber amplifiers (EDFA) used in our experiments. The pumps were amplified, band-pass filtered (BPF), and then synchronized and combined by wavelength division multiplexer (WDM). The peak pump power was monitored with a detector and oscilloscope. A CW signal (S) at 1544nm was combined with pumps using 90/10 coupler. The polarization controllers (PC) and a polarizing beam splitter (PBS) were used to ensure that the beams are collinearly polarized. The light was coupled into the waveguide using polarization maintaining (PM) taper lens-tipped fiber aligned to the TE polarization, and coupled out of the waveguide using a lens-tipped single-mode fiber. The spectra were observed on the optical spectrum analyzer (OSA).

4.2.3 Results and Discussion

The peak pulse power before the waveguide for pumps P1 and P2 was 1.43 W and 1.56 W, respectively. Assuming equal coupling loss at input and output and neglecting the propagation loss, the calculated peak pump powers inside the waveguide were 572 mW and 624 mW.

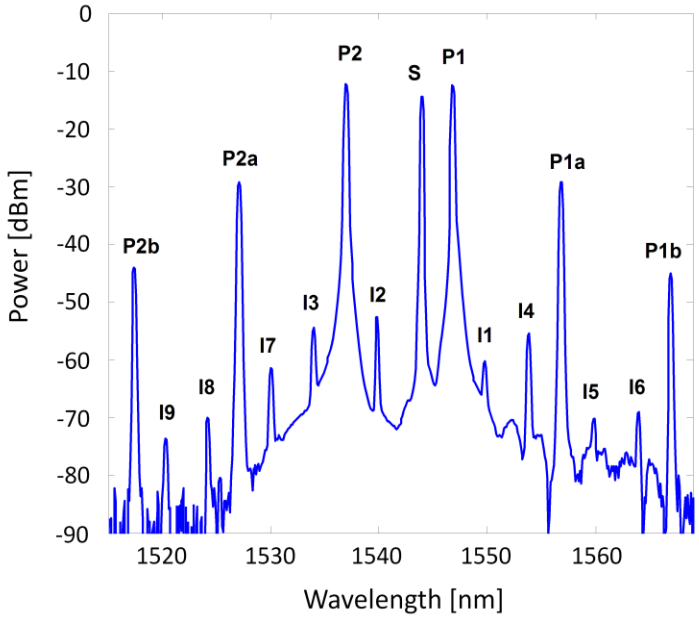

Figure 4.4: Measured two-pump FWM spectrum. Dual-pump FWM measurement shows first-order idlers I1-I3, and 9 total idlers generated from self-seeded higher-order pumps. Maximum conversion efficiency was -8.18 dB of I2.

The two-pump four-wave mixing spectrum of an 850 nm wide waveguide is shown in Fig 4.4. We clearly observe generation of the first order idlers I1, I2, and I3. In addition, mixing of the two pumps P1 and P2 produces self-seeded higher order pumps, P1b, P2a, and P2b, which act as addition pumps producing higher order idlers I4-I9. This represents a total of ten sidebands produced from an initial two pumps and signal, due to the generation of higher-order pumps. In order to determine the conversion efficiency, 30 dB is subtracted from the CW signal power to account for 0.1% duty cycle of the pumps. The conversion efficiencies between the signal and idlers I1, I2 and I3 are -15.8 dB, -8.18 dB and -10.34

dB, respectively. The signal is most efficiently converted into its phase-conjugated idler I2, while the modulation instability copy I1 has the lowest conversion efficiency. In comparison to the single pump parametric conversion efficiency of -5.7 dB on the same waveguide (Fig.2b), idler I1 power decreased by -10 dB, which is attributed to lower total pump power than in a single pump case, as well as energy redistribution between several four-wave mixing processes producing multiple sidebands.

4.3 Nondegenerate Two-Photon Absorption

The most important limitation of silicon nonlinear devices is pump power impairment due to nonlinear absorption caused by two-photon absorption (TPA) and the resulting free-carrier absorption (FCA) [14]. Even though the silicon band gap (1.11 eV) is larger than the photon energy for near-IR wavelengths and longer, two photons can be simultaneously absorbed through TPA to induce an electronic transition from the valence band to the conductance band (Fig 4.5). These excited free carriers can then absorb light through FCA.

The TPA-induced transition rate R scales with the square of the optical intensity I^2 [15]

$$R = \frac{\sigma}{\hbar\omega} I = \frac{\sigma^{(2)}}{\hbar\omega} I^2 \tag{4.6}$$

where the absorption cross section is linear with intensity $\sigma = \sigma^{(2)} I$ (and $\sigma^{(2)}$ is a coefficient that describe the strength of the TPA process). Thus, nonlinear absorption is always a concern for silicon FWM as it limits the pump power available for the mixing process. Indeed, to date both Raman gain and parametric gain in silicon waveguides have only been achieved using by avoiding the effects of nonlinear absorption by using ultra-short pump pulses [1, 13, 16], using active carrier sweep-out methods [17], or in the mid-infrared spectral region [14, 18]. To our knowledge, and as mentioned in Chapter 3, the high CW conversion efficiency achieved in silicon is -5.5 dB [19]. CW operation is generally required for communications and signal processing applications in contrast to ultra-short pump pulses, and high bias voltages for carrier sweep out are

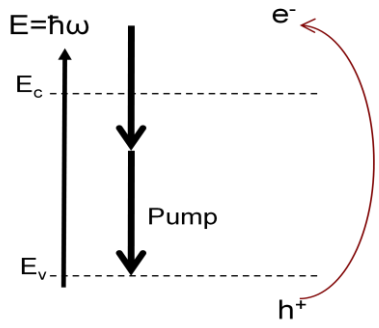

Figure 4.5: Two-photon absorption process illustration. At high pump intensities, two photons can be simultaneously absorbed to generate an electron-hole pair.

undesirable for compact integrated devices. It is thus vital to consider the impact of TPA on silicon device performance.

For two-pump FWM, nonlinear absorption is especially important if the nondegenerate TPA rate (one photon from each of two pumps are absorbed) differs than that of the degenerate TPA rate (two photons from one pump are absorbed). If the nondegenerate TPA rate is less than the degenerate TPA rate, then two-pump FWM should have improved conversion efficiency and parametric gain than with a single pump. Conversely, if the nondegenerate TPA rate is greater than the degenerate TPA rate, than two-pump FWM will suffer in terms of total pump power, and thus, parametric conversion efficiency.

The nondegenerate and degenerate TPA rates are compared using analytical equations [20]. For two waves with intensities I_1 and I_2, absorption due to cross (nondegenerate) TPA is given by

$$\frac{\partial}{\partial z} I_1 = -\omega_1 \beta_{TPA} I_1 I_2 \tag{4.7a}$$

$$\frac{\partial}{\partial z} I_2 = -\omega_2 \beta_{TPA} I_1 I_2 \tag{4.7b}$$

where β_{TPA} is the TPA coefficient. It is assumed that an equal number from each pumps are absorbed such that

$$\frac{1}{\omega_1}\frac{\partial}{\partial z}I_1 = \frac{1}{\omega_2}\frac{\partial}{\partial z}I_2 \ . \tag{4.8}$$

Another underlying assumption (as is assumed in ref. 20) is that the TPA coefficient β_{TPA} is the same for both the degenerate and nondegenerate case. The expressions (4.7) can be integrated, giving

$$I_1(z) = \frac{\omega_1 K^{'} I_{10}}{I_{10} - (\omega_1/\omega_2) I_{20} \exp\left(-\gamma \omega_1 \omega_2 K^{'} z\right)} \tag{4.9a}$$

$$I_2(z) = \frac{\omega_2 K^{'} I_{10}}{(\omega_2/\omega_1) I_{10} \exp\left(\gamma \omega_1 \omega_2 K^{'} z\right) - I_{20}} \tag{4.9b}$$

where $K^{'} = (I_1/\omega_1) - (I_2/\omega_2)$. In the degenerate (single-pump) case, where $\omega_1 = \omega_2 \equiv \omega$, then expression 4.7 becomes

$$\frac{\partial}{\partial z} I = \omega \gamma I^2 \tag{4.10}$$

with the solution

$$I(z) = I_0(1 + \omega \gamma I_0 z). \tag{4.11}$$

The nondegenerate (4.9) and degenerate (4.11) solutions are plotted in Fig. 4.6. These solutions show that in comparison to a single pump, the

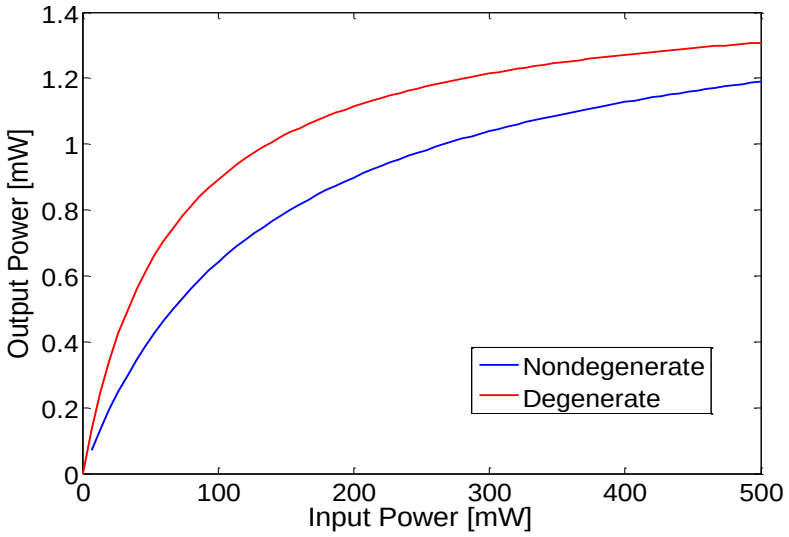

Figure 4.6: Comparison of degenerate and nondegenerate TPA. Calculated absorption using analytic equations show stronger pump power impairment due to TPA from nondegenerate TPA compared to the single-pump case.

nondegenerate cross-TPA of two pumps with the same total pump power is stronger. Thus, the multiple sideband generation provided by two-pump FWM comes with the trade-off of higher nonlinear absorption and lower conversion efficiency. The increased cross-TPA rate over the degenerate (self) TPA rate has been predicted previously, and even utilized for such applications as measuring the temporal characteristics of ultra-short pulses through autocorrelation and for ultrafast optical switching [21]. For FWM applications, however, this is a fundamental limitation to the performance of silicon devices as dual-pump or multiple-pump parametric nonlinear mixers.

4.4 Summary and Conclusion

FWM in silicon waveguides using dual pumps has been experimentally demonstrated. The dual pumps combined with generated higher-order pumps produced a total of ten sidebands, with a maximum conversion efficiency of -8.18 dB. Lower conversion efficiency compared to single-pump FWM was observed. This is explained by nondegenerate cross-TPA, which imposes a trade-off between the multiple sideband generation provided by dual pumps and the maximum attainable conversion efficiency compared to with a single pump.

REFERENCES

[1] M. A. Foster, A. C. Turner, J. E Sharping, B. S. Schmidt, M. Lipson, A. L. Gaeta, "Broad-band optical parametric gain on a silicon photonic chip," *Nature*, **441**, 960 (2006)

[2] D. R. Solli, J. Chou, B. Jalali, "Amplified wavelength-time transformation for real-time spectroscopy," Nature Photonics, 2 (1), 48 (2008)

[3] M. A. Foster, R. Salem, Y. Okawachi, A. C. Tuner-Foster, M. Lipson, A. L. Gaeta, "Ultrafast waveform compression using a time-domain telescope," *Nature Photonics*, **3**, 581 (2009)

[4] C. S. Brés, A. O. J. Wiberg, B. P. P. Kuo, J. M. Chavez-Boggio, C. F. Marki, N. Alic, S. Radic, "Optical demultiplexing of 320 Gb/s to 8-times-40 Gb/s in a single parametric gate," *Journal of Lightwave Technology*, **28** (4), 434 (2010)

[5] A. O. J. Wiberg, C. S Brés, B. P. P. Kuo, J. X. Zhao, N. Alic, S. Radic, "Sampling of Multiple 320-Gb/s Channels by Single Parametric Gate," *IEEE Photonics Technology Letters*, **21** (12), 796 (2009)

[6] J. M. Chavez-Boggio, J. D. Marconi, S. R. Bickham, H. L. Fragnito, "Spectrally flat and broadband double-pumped fiber optical parametric amplifiers," *Optics Express*, **15** (9), 5288-5309 (2007)

[7] C. S. Brés, A. O. J. Wiberg, B. P. P. Kuo, J. M. Chavez-Boggio, C. F. Marki, N. Alic, S. Radic, "Optical demultiplexing of 320 Gb/s to 8-times-40 Gb/s in a single parametric gate," *Journal of Lightwave Technology*, **28** (4), 434 (2010)

[8] A. O. J. Wiberg, C. S. Brés, B. P. P. Kuo, J. M. Chavez-Boggio, N. Alic, S. Radic, "Multicast parametric synchronous sampling of 320-Gb/s return-to-zero signal," *IEEE Photonics Technology Letters*, **21** (21), 1612 (2009)

[9] A. C. Turner-Foster, M. A. Foster, R. Salem, A. L. Gaeta, M. Lipson, "Frequency conversion over two-thirds of an octave in silicon nanowaveguides," *Optics Express*, **18** (3), 1904 (2010)

[10] A. Biberman, B. G. Lee, K. Bergman, A. C. Turner-Foster, M. Lipson, M. A. Foster, A. L. Gaeta, "First Demonstration of On-Chip Wavelength Multicasting," *Optical Fibers Conference* (IEEE/OSA, San Diego, CA, 2009)

[11] S. Radic, C. J. McKinstrie, "Two-pump fiber parametric amplifiers," *Optical Fiber Technology*, **9**, 7-23 (2003)

[12] C. J. McKinstrie, S. Radic, A. R. Chraplyvy, "Parametric amplifiers driven by two pump waves," *Journal of Selected Topics in Quantum Electronics*, **8** (3), 538-547 (2002)

[13] O. Boyraz, B. Jalali, "Demonstration of a silicon Raman laser," *Optics Express*, **12** (21), 5269 (2004)

[14] X. Liu, R. M. Osgood, Y. A. Vlasov, W. M. J. Green, "Mid-infrared optical parametric amplifier using silicon nanophotonic waveguides," *Nature Photonics*, **4** (8), 557 (2010)

[15] R. Boyd, *Nonlinear Optics*, 3rd Ed, Academic Press, Burlington, MA, 2008

[16] H. Rong, S. Xu, O. Cohen, O. Raday, M. Lee, V. Sih, M. Paniccia, "A cascaded silicon Raman laser," *Nature Photonics*, **2** (3), 170 (2008)

[17] H. Rong, R. Jones, A. Liu, O. Cohen, D. Hak, A. Fang, M. Paniccia, "A continuous-wave Raman silicon laser," *Nature*, **433**, 725 (2005)

[18] V. Raghuanathan, D. Borlaug, R. R. Rice, B. Jalali, "Demonstration of a mid-infrared silicon Raman Amplifier," *Optics Express*, **15** (22), 14355 (2007)

[19] W. Mathlouthi, H. Rong, M. Paniccia, "Characterization of efficient wavelength conversion by four-wave mixing in sub-micron silicon waveguides," *Optics Express*, **16** (21), 16735 (2008)

[20] Y. R. Shen, *Principles of Nonlinear Optics*, Wiley, Hoboken, NJ (1984)

[21] Q. Lin, O. J. Painter, G. P. Agrawal, "Nonlinear optical phenomena in silicon waveguides: modeling and applications," *Optics Express*, **15** (25), 16604 (2007)

Chapter 4 contains, in part, material presented at:

- J. S. Park, S. Zlatanovic, M. L. Cooper, J. M. Chavez-Boggio, I. B. Divliansky, N. Alic, S. Mookherjea, S. Radic, "Two-Pump Four-Wave Mixing in Silicon Waveguides," *Frontiers in Optics: OSA 93rd Annual Meeting*, FML2, San Jose, 2009

The dissertation author was the primary author of the paper.

5. MID-INFRARED FOUR-WAVE MIXING IN SILICON WAVEGUIDES

5.1 Introduction

Mid-infrared (mid-IR) light sources are essential for applications that include free-space communication, chemical and biomolecular sensing, and infrared spectroscopy [1-4, 21, 22], yet no devices comparable to those in the near-infrared (NIR) have emerged to date. Lasers operating above 1.8 μm, including optical parametric oscillators, thulium-doped fiber lasers, quantum cascade lasers do not combine large tunable range, narrow linewidth, and generally cannot be modulated to support advanced applications [5, 6]. Quantum cascade lasers hold promise for wide tunability and direct modulation, but require active thermal management [7, 8].

Wavelength conversion in a mid-IR transparent material such as silicon offers a promise for an ultra-compact mid-IR source that combines wide wavelength tuning, narrow linewidth, and arbitrarily complex modulation rivaling those in the near-IR telecommunications window. Here we report FWM in silicon waveguides in the spectral region beyond 2 μm using pump and probe waves derived from compact and telecom-compatible near-IR fiber-optic sources. We measure a high value of the

nonlinear parameter γ = 97.3 $(Wm)^{-1}$ and achieve four-wave mixing over a bandwidth of 630 nm, achieving generation of a record long wavelength on a silicon chip of up to 2388 nm from a first-order (single-step) conversion.

This dissertation thus far has reviewed and presented a range of efforts in place towards engineering SOI parametric devices for communications and signal processing applications. While these devices are bound by trade-offs between high nonlinearity and high nonlinear absorption, the spectral region beyond 2 μm is of interest for silicon FWM since two-photon absorption (TPA) and the resulting free-carrier absorption (FCA) are reduced as the combined energy of two photons becomes less than the band-gap energy of silicon. Thus, silicon could potentially be an attractive platform for parametric nonlinear optics where a mid-IR source is critical for application such as LIDAR, atmospheric communication, chemical and bio-molecular sensing, and infrared spectroscopy. Recently, four-wave mixing near the 2.2 μm TPA threshold wavelength has been demonstrated with picosecond pump pulses generated from a Ti:sapphire laser-pumped optical parametric oscillator (OPO) with peak pump power exceeding 20 W coupled into large-area (700 nm x 425 nm) silicon waveguides [9, 23]. Unfortunately, conventional OPO pumping is not compatible with the ultimate goal for

compact, low power, and cascadable parametric devices. In addition, the picosecond-long pulses do not fully utilize the advantage of reduced TPA and FCA at 2 μm [10], and provide limited functionality in communication and sensing applications. To address these critical limitations, we have investigated the feasibility of a low power mid-IR silicon nonlinear parametric mixer that driven by telecom compatible sources.

Consequently, we demonstrate a low-power mid-IR silicon parametric mixer using a quasi-CW pump generated by telecom-compatible fiber light sources. FWM was performed with long pump pulses whose duration (1 ns) was comparable to the free carrier lifetime in silicon to measure the nonlinear parameter γ of 97.3 $(Wm)^{-1}$ at 2.025 μm, consistent with previous measurements at TPA threshold wavelengths [9, 23]. These results demonstrate the viability of silicon as a mid-IR nonlinear optics platform without the need for specialized and costly infrared pump sources. The fiber-based source can be spooled to a millimeter-scale radius, as illustrated in Fig 1b, allowing each element of the mid-IR source architecture to have a compact size. Combined with standard pumping diodes, this source maintains an ultra-compact footprint while providing bandwidth and continuous tuning range not achievable with silicon mid-IR Raman-based devices [3, 4].

5.1.1 Silicon Nonlinearities in the Mid-Infrared

Silicon may become the preferred material of choice for integrated photonic and optoelectronic devices in the mid-infrared for a variety of reasons, including low linear absorption up to ~6 μm, increased free-carrier plasma effect compared to NIR, ease of fabrication, and compatibility with a wide range of applications including atmospheric and free-space communications and spectroscopy [2]. The development of nonlinear optical devices in the mid-infrared would add important all-optical signal processing capabilities. To date, characterization of the optical nonlinearities silicon has been limited to bulk measurements only near the TPA threshold wavelength [11, 12] or relatively simply absorption measurements [13]. The Kerr coefficient is expected to decrease at longer mid-infrared wavelengths compared to the NIR telecommunications window [11, 12]. Further, more thorough work to accurately quantify this decrease has yet to emerge. However, the reduction or absence of nonlinear absorption indicates an overall improvement in the nonlinear figure of merit (FOM) $n_2/\lambda\beta_{TPA}$, and we demonstrate here (along with others [9, 23]) the feasibility of mid-infrared parametric devices.

5.2 Fiber-Optic-Based Mid-Infrared Source

A point of concern for all areas of silicon photonics is the lack of on-chip light sources. In the near-IR region, this has been addressed either by the heterogeneous integration of III-V materials onto the silicon chip [14] or by engineering efficient coupling from off-chip sources [15]. The practicality of these approaches comes from the wide availability of affordable lasers and amplifiers at NIR wavelengths, including electrically pumped semiconductor lasers and amplifiers and erbium-doped fiber amplifiers, thanks to a tremendous amount of development driven by the telecommunications industry. However, there is currently a lack of sources in the mid-IR spectral range which combine compact size, affordable cost, and wide tuning range. OPOs can reach mid-IR wavelengths with high peak power, but are generally pumped by mode-locked lasers which are large in size, generally limited to ultra-short pulses, require precise alignment and a stable operating environment, and are costly. Quantum cascade lasers (QCL) have been demonstrated with wide tuning range in the mid-IR, but room temperature operation in the 3-4 μm range presents a challenge due to materials limitations [7]. Thulium-doped fiber lasers and amplifiers can provide high power but have only very narrow range near 1.9 to 2 μm [16]. Considering that two key advantages of silicon photonics are low-cost manufacturing using existing CMOS

fabrication and dense integration in a compact package, the need for costly and/or bulky pump sources offsets these advantages while limiting many potential applications.

Practically, a great deal of effort in developing these specialized laser sources can be saved if instead, well-developed near-IR sources can be directly translated to the mid-IR spectral region. Parametric wavelength conversion from the near-IR into mid-IR wavelengths can provide this capability, provided a suitable parametric mixing platform is available. Such wide-band wavelength conversion has been demonstrated in highly-nonlinear fiber (HNLF) [17], and offers an approach in which not only light generation and amplification, but data modulation technology developed for the telecom industry can be directly applied to mid-IR applications. Not only does parametric conversion in HNLF provide a means of mid-IR light generation using widely-available off-the-shelf components, but also one that is compact and package-able into a small form. The HNLF used in our experiments can be spooled to a millimeter-scale radius with negligible bend loss for wavelengths up to 2.3 μm (Fig. 5.Ib) [20], showing tremendous promise for an ultra-compact pump source to be used in conjunction with chip-scale silicon mid-IR devices (Fig. 5.1c). Here we explore the feasibility of using a fiber-based mid-IR source for silicon nonlinear optics applications.

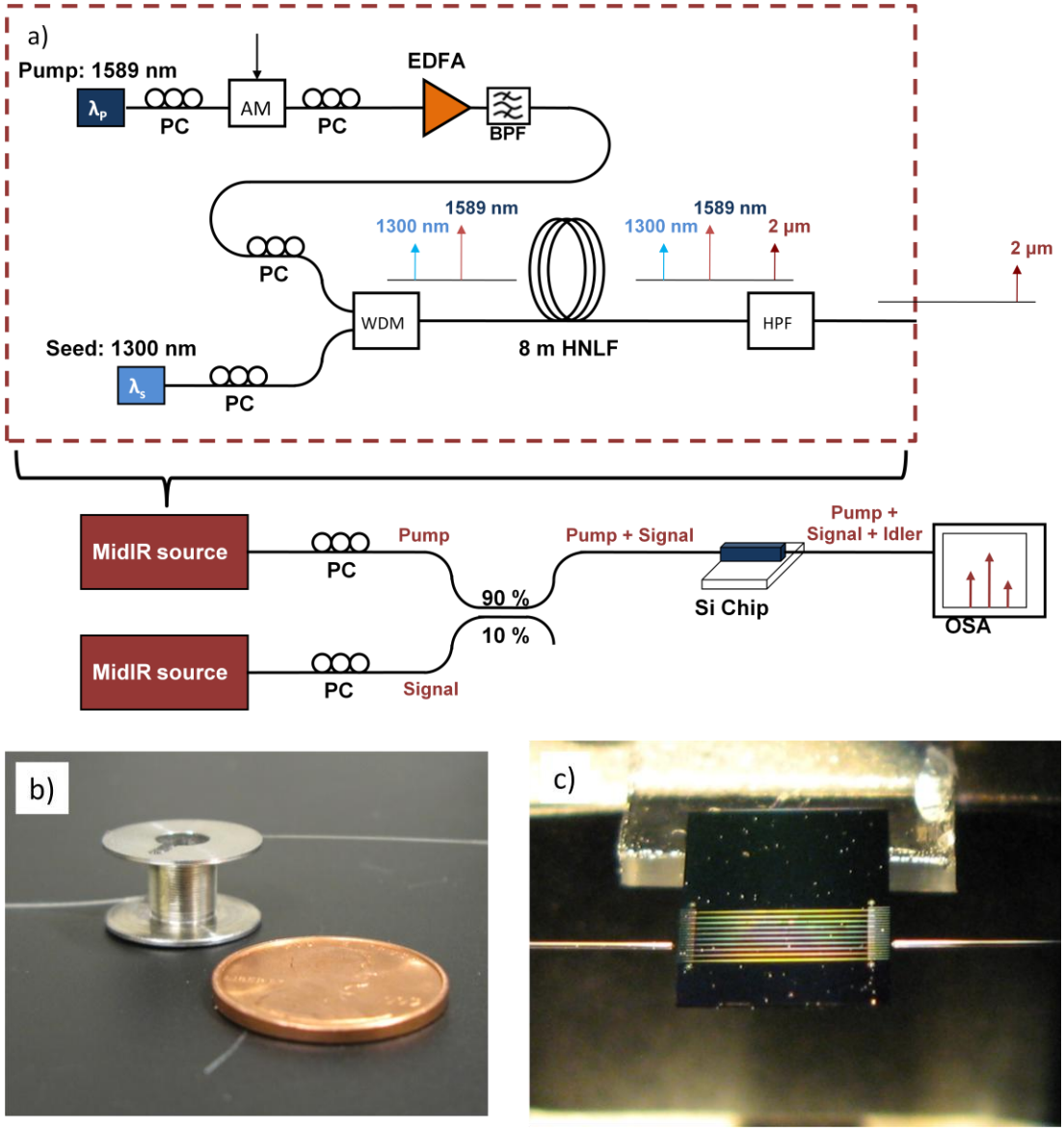

Figure 5.1: Mid-IR FWM setup and fiber and silicon parametric mixers. a) Schematic of the measurement setup. Abbreviations: PC: polarization controller, EDFA: erbium-doped fiber amplifier, BPF: band pass filter, WDM: wavelength division multiplexer, HNLF: highly-nonlinear fiber, HPF: high pass filter, OSA: optical spectrum analyzer. b) size limitation of fiber-based mid-IR source. c) SOI chip with input and output fibers aligned.

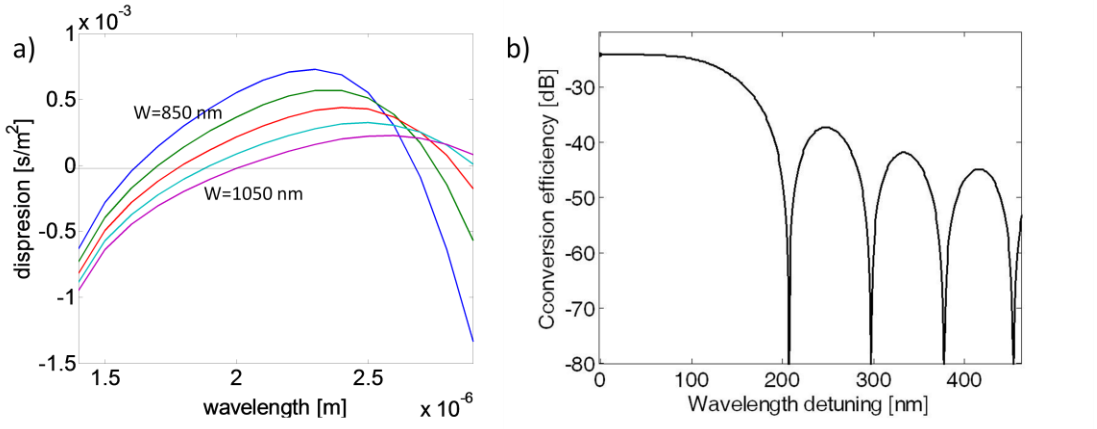

Figure 5.2: Calculated dispersion and FWM spectrum. a) Calculated dispersion for waveguides of 250 nm height and various widths from 850 nm to 1050 nm in 50 nm increments. b) Calculated FWM spectrum for the 1060 nm wide waveguide used in our experiments.

The schematic of our experiment is shown in Fig. 5.Ia. A pump laser at 1589 nm (Santec external cavity laser) is amplitude modulated to produce 1 ns pulses with a 1 MHz repetition rate, then amplified by a 3-stage EDFA. The amplified pump is spectrally filtered to removed amplified spontaneous emission (ASE) noise, then combined with a seed laser at 1309 nm and inserted into 8 m of HNLF. Parametric mixing in the HNLF produces an idler at 2025 nm. The peak power of the 1589 pump is ~53 dBm, and the 10 dBm of 1309 nm seed power is converted with 20 dB of conversion gain to 30 dBm peak power at 2025 nm. The 1589 nm and 1309 nm seed are high-pass-filtered, leaving the generated 2025 nm idler to be used as a Mid-IR pump for silicon FWM. A second identical setup, seeded

by a tunable laser from 1260 nm to 1360 nm is used as a tunable Mid-IR signal from near the pump wavelength down to 1912 nm.

5.3 Mid-IR Four-Wave Mixing

The silicon waveguides were fabricated using the process described in Chapter 3. The cross sectional dimensions were 1060 nm x 250 nm (width x height) and were 3.8 mm in length. The input and output inverse tapers were overlaid with SU-8 polymer waveguides using the same process described. The total fiber-to-fiber insertion loss at 2025 nm was 15 dB. We assumed similar propagation loss as measured in Chapter 3 (~2.8 dB/cm), due to lower scattering at longer wavelengths [18]. Thus, the estimated total propagation loss was ~1 dB. The high coupling loss at 2 μm is primarily due to poor mode matching between the input and output lens-tipped fibers and the polymer waveguide input and outputs. The calculated dispersion and FWM response are shown in Fig. 5.2.

The Mid-IR pump and signal sources described in the previous section were combined using a 90/10 fiber coupler, and then coupled into the silicon waveguides with a lens-tipped fiber described in Chapter 3. The waveguide output was fiber-coupled, and observed on an extended-range OSA capable of measuring up to 2.4 μm. Figure 5.3a shows the measured FWM spectra with the pump at 2025 nm, the seed

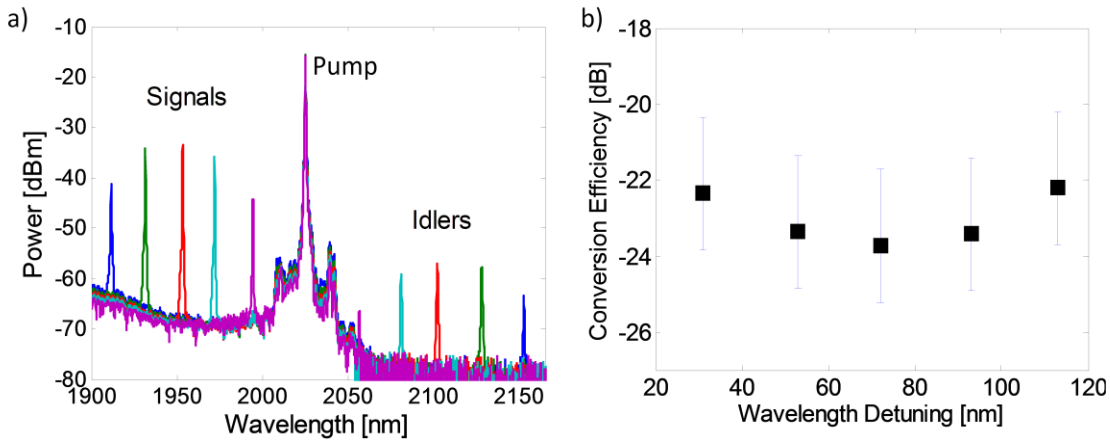

Figure 5.3: Mid-IR FWM measurements. a)Measure FWM spectra across a range of 241 nm. b) Measured conversion efficiency vs. pump-signal wavelength detuning, showing 2 dB-equalized conversion over the measured range.

tuned from 2 μm to 1912 nm, and the generated idlers. The measured conversion efficiency, plotted in Figure 5.3b as a function of pump-probe wavelength detuning, had a peak value of -22.2 dB and was 2 dB equalized across the entire measured range of 241nm (this measurement range was limited only by the availability of a seed laser beyond 1360 nm). By assuming reciprocal and equal input and output coupling efficiencies, the peak pump power inside the waveguide was calculated to be 176 mW. Theoretical prediction of conversion efficiency computed for the waveguide dimensions, pump wavelength and power used in our

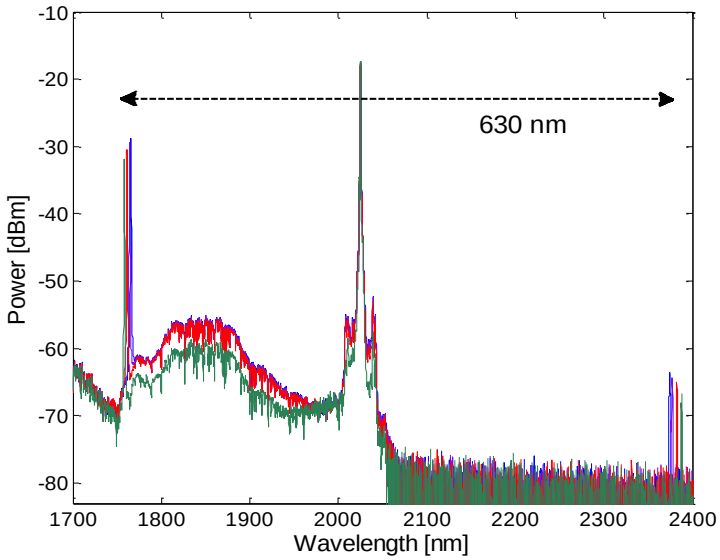

Figure 5.4: 630nm-wide conversion to 2388 nm. Maximum achieved FWM bandwidth shows generation of 2388 nm light in a first-order FWM conversion.

experiments (Figure-5.2b) showed expected conversion bandwidth of 292 nm.

The maximum parametric conversion bandwidth was measured by generating a probe at 1758 nm with a 1450 nm seed in HNLF, and subsequent mixing with the 2025 nm pump in the silicon waveguide to produce an idler at 2388 nm, as shown in Figure 5.4. Accounting for the measured loss of the output silica fiber at this idler wavelength, the efficiency of -36.8 dB was measured for 630 nm conversion process. To the best of our knowledge, this is the longest infrared wavelength generated by a first order FWM conversion process in a silicon chip [19].

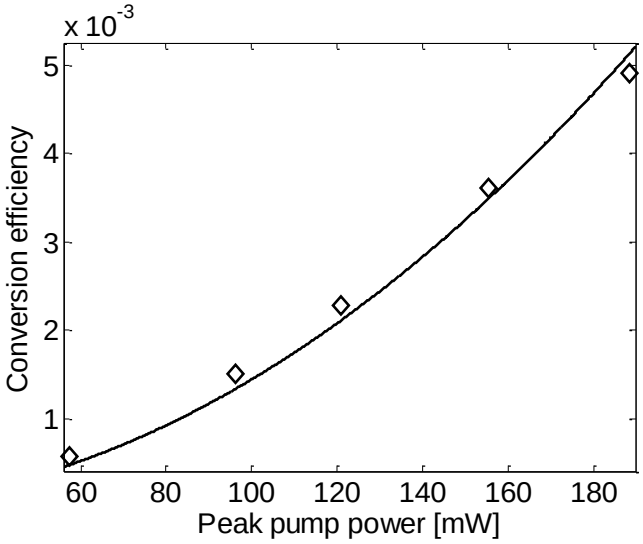

Figure 5.5: Conversion efficiency vs. pump power. The nonlinearity coefficient γ was estimated by fitting the measured conversion efficiency as a function of pump power.

To quantify the nonlinearity coefficient γ, we measured conversion efficiency dependence on pump power (Figure 5.5) and extracted the coefficient by fitting the curve with expected dependence of the conversion efficiency G on pump power P_0,

$$G(P_0) = (\gamma P_0/g)^2 * sinh^2(gL), \tag{5.1}$$

where L is waveguide length, $g = \sqrt{(\gamma P_0)^2 - \left(\frac{\Delta k + 2\gamma P_0}{2}\right)^2}$ and $\Delta k = 2\pi(n_s/\lambda_s + n_i/\lambda_i - 2n_p/\lambda_p)$, and n_s, n_i, and n_p are effective indices at signal, idler and pump wavelength, respectively, obtained from finite

element simulations. Conversion efficiency was measured from the spectra, while the input peak pump power was obtained by adding output coupler and propagation loss to average power and 30dB to account for 1:1000 pulsing duty-cycle. The value of γ obtained was 97.3 $(Wm)^{-1}$.

5.4 Summary and Conclusion

In conclusion, we demonstrate mid-infrared four-wave mixing in silicon waveguides with a 2 μm pump generated from telecom-compatible fiber-optic source. The measurements indicate that the nonlinear parameter γ is comparable to that in the NIR band near 1550 nm, and combined with reduction in TPA-induced nonlinear absorption yields a ten-fold improvement in nonlinear FOM. In contrast to previous attempts to generate 2 μm light in silicon waveguides using pump near 1550 nm [19], this approach is not limited by nonlinear absorption of the pump, and is thus scalable by engineering of the silicon waveguides and infrared source. Consequently, a two-stage parametric mixer that combines NIR (silica) and Mid-IR (silicon) waveguides holds a considerable potential for wide range of mid-infrared nonlinear optic devices.

REFERENCES

[1] M. Ebrahim-Zadeh, I. T. Sorokia (Ed.), *Mid-Infrared Coherent Sources and Applications* (Springer, Dordrecht, 2008)

[2] R. A. Soref, S. J. Emelett, W. R. Buchwald, "Silicon waveguided components for the long-wave infrared," *Journal of Optics A: Pure and Applied Optics*, **8**, 840 (2006)

[3] V. Raghuanathan, D. Borlaug, R. R. Rice, B. Jalali, "Demonstration of a mid-infrared silicon Raman Amplifier," *Optics Express*, **15** (22), 14355 (2007)

[4] H. Rong, S. Xu, O. Cohen, O. Raday, M. Lee, V. Sih, M. Paniccia, "A cascaded silicon Raman laser," *Nature Photonics*, **2** (3), 170 (2008)

[5] S. Kameyama, M. Imaky, Y. Hirano, S. Ueno, S. Kawakami, D. Sakaizawa, M. Nakajima, "Development of 1.6 μm continuous-wave modulation hard-target differential absorption LIDAR system for CO_2 sensing," *Optics Letters*, **34**, 1513 (2009)

[6] M. Bashkansky, H. R. Burris, E. E. Funk, R. Mahon, C. I. Moore, "RF phase-encoded random-modulation LIDAR," *Optics Communicatios*, **231**, 93 (2004)

[7] G. Wysocki, R. Lewicki, R. F. Curl, F. K. Tittel, L. Diehl, F. Capasso, M. Troccoli, G. Hofler, D. Bour, S. Corzine, R. Maulini, M. Giovanni, J. Faist, "Widely tunable mode-hop free external cavity quantum cascade lasers for high resolution spectroscopy and chemical sensing," *Applied Physics B*, **92** (3), 305 (2008)

[8] G. Hancock, J. H. van Helden, R. Peverall, G. A. D. Ritchie, R. J. Walker, "Direct and wavelength modulation spectroscopy using a CW external cavity quantum cascade laser," *Applied Physics Letters*, **94**, 201110 (2009)

[9] X. Liu, R. M. Osgood, Y. A. Vlasov, W. M. J. Green, "Broadband mid-infrared parametric amplification, net off-chip gain, and cascaded four-wave mixing in silicon photonic wires," *6th International Conference on Group IV Photonics* (IEEE, San Francisco, CA, 2009)

[10] M. A. Foster, A. C. Turner, J. E Sharping, B. S. Schmidt, M. Lipson, A. L. Gaeta, "Broad-band optical parametric gain on a silicon photonic chip," *Nature*, **441**, 960 (2006)

[11] Q. Lin, J. Zhang, G. Piredda, R. W. Boyd, P. M. Fauchet, G. P. Agrawal, "Dispersion of silicon nonlinearities in the near infrared region," *Applied Physics Letters*, **91**, 021111 (2007)

[12] A. D. Bristow, N. Rotenberg, H. M. van Driel, "Two-photon absorption and Kerr coefficients of silicon for 850 – 2200 nm," *Applied Physics Letters*, **90**, 191104 (2007)

[13] V. Raghunathan, R. Shori, O. M. Stafsudd, B. Jalali, "Nonlinear absorption in silicon and the prospects of mid-infrared silicon Raman Lasers," *Physica Status Solidi (a)*, **203** (5), R38 (2006)

[14] A. W. Fang, H. Park, O. Cohen, R. Jones, M. J. Paniccia, J. E. Bowers, "Electrically pumped hybrid AlGaInAs-silicon evanescent laser," *Optics Express*, **14** (20), 9203 (2006)

[15] S. J. McNab, N. Moll, Y. A. Vlasov, "Ultra-low loss photonic integrated circuit with membrane-type photonic crystal waveguides," *Optics Express*, **11** (22), 2927 (2003)

[16] L. E. Nelson, E. P. Ippen, H. A. Haus, "Broadly tunable sub-500 fs pulses from an additive-pulse mode-locked thulium-doped fiber ring laser," *Applied Physics Letters*, **67** (1), 19 (1995)

[17] J. M. Chavez-Boggio, S. Moro, B. P. P. Kuo, N. Alic, B. Stossel, S. Radic, "Tunable parametric all-fiber short-wavelength IR transmitter," *Journal of Lightwave Technology*, **28** (4), 443 (2010)

[18] L. E. Busse, G. H. McCabe, I. D. Aggarwal, "Wavelength dependence of the scattering loss in fluoride optical fibers," *Optics Letters*, **15**, 423 (1990)

[19] A. C. Turner-Foster, M. A. Foster, R. Salem, A. L. Gaeta, M. Lipson, "Frequency conversion over two-thirds of an octave in silicon nanowaveguides," *Optics Express*, **18** (3), 1904 (2010)

[20] J. M. Chavez-Boggio, S. Zlatanovic, F. Gholami, J. M. Aparicio, S. Moro, K. Balch, N. Alic, S. Radic, "Short wavelength infrared frequency conversion in ultra-compact fiber device," *Optics Express*, **18** (2), 439 (2010)

[21] R. Soref, "Mid-infrared photonics in silicon and germanium," *Nature Photonics*, **4** (8), 495 (2010)

[22] B. Jalali, "Silicon Photonics: Nonlinear optics in the mid-infrared," *Nature Photonics*, **4** (8), 506 (2010)

[23] X. Liu, R. M. Osgood, Y. A. Vlasov, W. M. J. Green, "Mid-infrared optical parametric amplifier using silicon nanophotonic waveguides," *Nature Photonics*, **4** (8), 557 (2010)

Chapter 5 contains material published in:

- S. Zlatanovic, J. S. Park, S. Moro, J. M. Chavez-Boggio, I. B. Divliansky, N. Alic, S. Mookherjea, S. Radic, "Mid-Infrared Wavelength Conversion in Silicon Waveguides Using Ultra-Compact Telecom-Band-Derived Pump Source," *Nature Photonics*, **4** (8), 561 (2010)
- J. S. Park, S. Zlatanovic, S. Moro, J. M. Chavez-Boggio, I. B. Divliansky, S. Mookherjea, S. Radic, "Mid-Infrared Four-Wave Mixing in Silicon Waveguides Using Telecom-Compatible Light Sources," *Frontiers in Optics: OSA 93rd Annual Meeting*, PDPB3, San Jose, 2009

The dissertation author is the co-primary author of the journal paper and was the presenter of the conference post-deadline session presentation.